




## RESEARCH ARTICLE

# Dopamine-conjugated extracellular vesicles induce autophagy in Parkinson's disease

Jae Hoon Sul<sup>1</sup> | Sol Shin<sup>2</sup> | Hark Kyun Kim<sup>1</sup>  | Jihoon Han<sup>1</sup>  | Junsik Kim<sup>1</sup> |  
 Soyong Son<sup>2</sup> | Jungmi Lee<sup>2</sup> | Seung Hyun Baek<sup>1</sup> | Yoonsuk Cho<sup>1</sup> | Jeongmi Lee<sup>1</sup> |  
 Jinsu Park<sup>3,1</sup> | Donghoon Ahn<sup>1</sup> | Sunyoung Park<sup>1</sup> | Leon F. Palomera<sup>1</sup> | Jeein Lim<sup>1</sup> |  
 Jongho Kim<sup>1</sup> | Chanhee Kim<sup>1</sup> | Seungsu Han<sup>4</sup> | Ka Young Chung<sup>1</sup> | Sangho Lee<sup>4</sup> |  
 Tae-in Kam<sup>5</sup> | Yunjong Lee<sup>6</sup> | Jeongyun Kim<sup>3</sup> | Jae Hyung Park<sup>2,3,7</sup>  |  
 Dong-Gyu Jo<sup>1,3,7,8</sup> 

<sup>1</sup>School of Pharmacy, Sungkyunkwan University, Suwon, Republic of Korea

<sup>2</sup>School of Chemical Engineering, College of Engineering, Sungkyunkwan University, Suwon, Republic of Korea

<sup>3</sup>Department of Health Sciences and Technology, SAIHST, Sungkyunkwan University, Suwon, Republic of Korea

<sup>4</sup>Department of Biological Sciences, Sungkyunkwan University, Suwon, Republic of Korea

<sup>5</sup>Department of Brain and Cognitive Sciences, Korea Advanced Institute of Science and Technology, Daejeon, Republic of Korea

<sup>6</sup>Department of Molecular Cell Biology, Sungkyunkwan University School of Medicine, Suwon, Republic of Korea

<sup>7</sup>Biomedical Institute for Convergence, Sungkyunkwan University, Suwon, Republic of Korea

<sup>8</sup>Institute of Quantum Biophysics, Sungkyunkwan University, Suwon, Republic of Korea

## Correspondence

Dong-Gyu Jo, School of Pharmacy, Sungkyunkwan University, Suwon, Republic of Korea. and Jae Hyung Park, School of Chemical Engineering, College of Engineering, Sungkyunkwan University, Suwon, Republic of Korea.  
 Email: jodg@skku.edu and jhpark1@skku.edu

## Funding information

National Research Foundation of Korea, Grant/Award Numbers: RS-2024-00345742, RS-2024-00399237, RS-2023-00256265; Korea Drug Development Fund, Grant/Award Numbers: RS-2021-DD121228, RS-2022-DD128953

## Abstract

The application of extracellular vesicles (EVs) as vehicles for anti-Parkinson's agents represents a significant advance, yet their clinical translation is hampered by challenges in efficient brain delivery and complex blood-brain barrier (BBB) targeting strategies. In this study, we engineered dopamine onto the surface of adipose-derived stem cell EVs (Dopa-EVs) utilizing a facile, two-step cross-linking approach. This engineering enhanced neuronal uptake of the EVs in primary neurons and neuroblastoma cells, a process shown to be competitively inhibited by dopamine pretreatment and dopamine receptor antibodies. Notably, Dopa-EVs demonstrated increased brain accumulation in mouse Parkinson's disease (PD) models. Therapeutically, Dopa-EVs administration led to the rescue of dopaminergic neuronal loss and amelioration of behavioural deficits in both 6-hydroxydopamine (6-OHDA) and  $\alpha$ -Syn PFF-induced PD models. Furthermore, we observed that Dopa-EVs stimulated autophagy evidenced by the upregulation of Beclin-1 and LC3-II. These findings collectively indicate that surface modification of EVs with dopamine presents a potent strategy for targeting dopaminergic neurons in the brain. The remarkable therapeutic potential of Dopa-EVs, demonstrated in PD models, positions them as a highly promising

Jae Hoon Sul and Sol Shin contributed equally to this study.

This is an open access article under the terms of the [Creative Commons Attribution-NonCommercial](https://creativecommons.org/licenses/by-nc/4.0/) License, which permits use, distribution and reproduction in any medium, provided the original work is properly cited and is not used for commercial purposes.

© 2024 The Author(s). *Journal of Extracellular Vesicles* published by Wiley Periodicals, LLC on behalf of the International Society for Extracellular Vesicles.

candidate for PD treatment, offering a significant advance over current therapeutic modalities.

#### KEYWORDS

autophagy, dopamine, exosome, extracellular vesicles, Parkinson's disease

## 1 | INTRODUCTION

Parkinson's disease (PD), the second most common neurodegenerative disease globally, is characterized by the progressive degeneration of dopaminergic neurons in the substantia nigra pars compacta (SNpc). This degeneration underlies the emergence of both motor and non-motor symptoms associated with the disease (Vázquez-Vélez & Zoghbi, 2021). Pathologically, PD is marked by the presence of intraneuronal protein aggregates known as Lewy bodies in post-mortem brain analyses (Spillantini et al., 1997). Despite two centuries of intensive research yielding invaluable insights, therapeutic strategies primarily revolve around dopamine replenishment, including dopamine receptor agonists and levodopa (L-DOPA), which remain the most effective treatment for PD patients (Carlsson et al., 1957; Charvin et al., 2018; McFarthing et al., 2020). In pursuit of a more fundamental treatment for PD, numerous clinical studies are underway exploring the transplantation of dopaminergic neurons derived from embryonic stem cells (Freed et al., 2001), and induced pluripotent stem cells (iPSCs) (Schweitzer et al., 2020). However, significant concerns about the safety, technical feasibility, and financial viability of these novel approaches persist (Gonzalez et al., 2015; Trounson & McDonald, 2015; Yamanaka, 2020).

Small extracellular vesicles (EVs), composed of the lipid bilayer and secreted by most cells and tissues, play a pivotal role as mediators of intercellular communication, transferring unique biological information from their cells of origin (Garcia-Martin et al., 2022; Gurung et al., 2021). Adipose-derived mesenchymal stem cells (ADSC), a subset of mesenchymal stem cells known for their multipotency and self-renewal capabilities, have emerged as a promising resource for regenerative therapies. EVs derived from ADSC (ADSC-EVs) have demonstrated protective effects in a variety of conditions including liver fibrosis (Han et al., 2020), cartilage degeneration (Woo et al., 2020), osteoporosis (Lee et al., 2021), ageing (Sanz-Ros et al., 2022), Alzheimer's disease (Lee et al., 2018), Huntington's disease (Lee et al., 2016), and amyotrophic lateral sclerosis (Lee et al., 2016). However, the specific role of ADSC-EVs in PD and their mechanisms in mitigating diverse neurodegenerative diseases remain to be fully elucidated.

Despite remarkable progress in the development of brain-targeting EVs, the challenges of inefficient and non-specific delivery within the brain have remained significant barriers to the clinical application of EVs in neurodegenerative diseases (Choi et al., 2022). Prior research has indicated the potential of receptor-mediated endocytosis for facilitating the translocation of EVs across blood-brain barrier (BBB) and specifically targeting brain pathologies (Kojima et al., 2018; Qu et al., 2018; Yang et al., 2021). However, these brain-targeting strategies are often complex and face obstacles due to the heterogeneous population of EVs, particularly when applying these techniques to already isolated EVs and those derived from biofluids. A recent innovation in this field involves the use of click-chemistry to efficiently functionalize the surface of EVs for brain targeting (Tian et al., 2018). Dopamine, is a critical neurotransmitter in the brain, and its receptors are extensively distributed throughout various brain regions. Particularly, dopamine receptor 2 (D2R), a subtype of dopamine receptors, is predominantly located in the basal ganglia, substantia nigra pars reticulata (SNr), and ventral tegmental area (VTA) (Burns et al., 2019). Previous research demonstrated that dopamine-conjugated nanoparticles significantly enhanced uptake in a dopamine receptor-dependent manner (Liu et al., 2021; Zhang et al., 2015). However, the feasibility of functionalizing dopamine on the surface of EVs and the efficacy of dopamine-conjugated EVs in targeting the brain in vivo remain unclear.

In this study, we introduced a novel method of EVs engineering to selectively target dopaminergic neurons in PD by conjugating dopamine onto the surface of ADSC-EVs using a straightforward and crosslinking reaction (Figure 1a). We found that intravenously administrated Dopa-EVs substantially increased brain accumulation in PD mice. Furthermore, these Dopa-EVs improved motor dysfunction and mitigated dopaminergic neuronal degeneration in 6-Hydroxydopamine (6-OHDA) and  $\alpha$ -synuclein preformed fibril ( $\alpha$ -Syn PFF)-induced PD models, primarily through the induction of autophagy (Figure 1b). These findings suggest that dopamine functionalization on EVs effectively targets dopaminergic neurons in PD, positioning Dopa-EVs as a promising strategy for this condition.

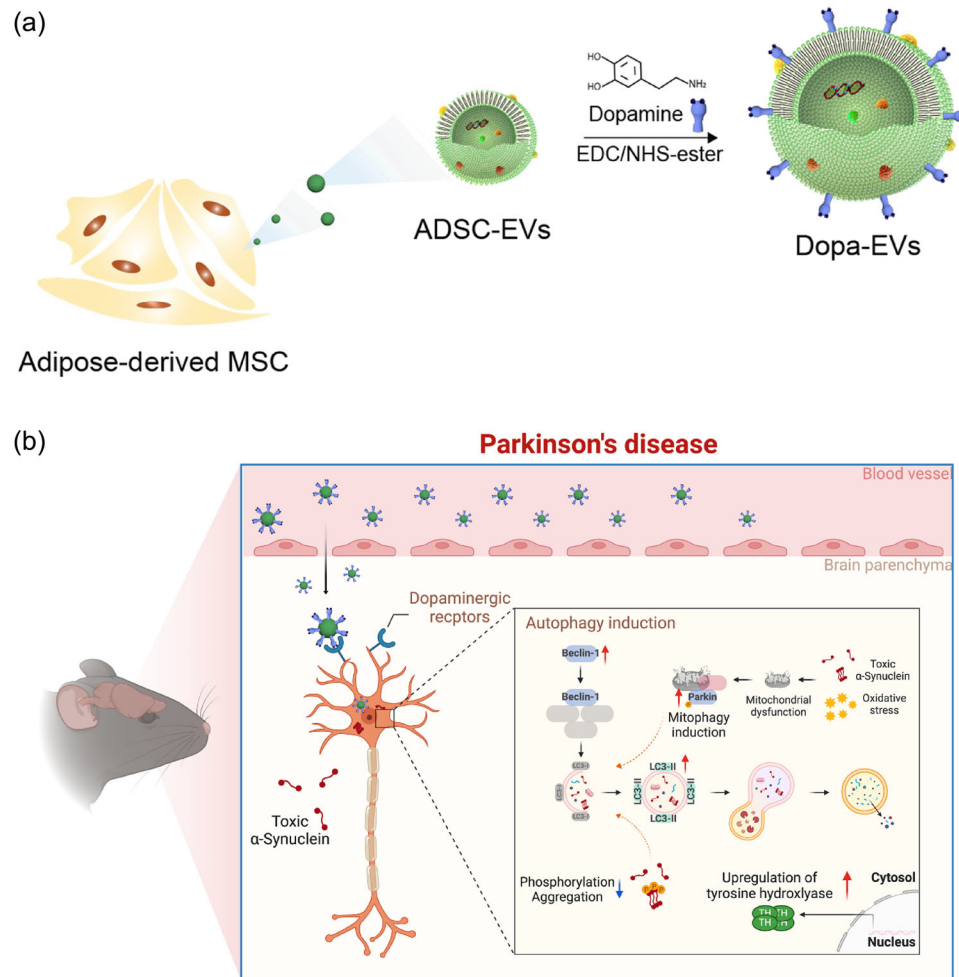


**FIGURE 1** Schematic illustration of dopamine engineered ADSC-EVs (Dopa-EVs) for brain-targeted delivery and their anti-Parkinson's mechanisms. (a) Dopamine was cross-linked onto the surface of the ADSC-EVs (Dopa-EVs) using EDC/NHS-ester. (b) Intravenous administration of Dopa-EVs selectively targeted dopaminergic neurons via dopamine receptor-mediated endocytosis leading to enhanced brain accumulation. Dopa-EVs stimulated autophagy induction by upregulation of Beclin-1, Parkin and LC3-II expression. Benefiting from this effect, Dopa-EVs treatment eliminated pathological  $\alpha$ -synuclein, upregulated TH expression, and improved dopaminergic neuronal loss and motor dysfunction in 6-hydroxydopamine and  $\alpha$ -synuclein-induced PD mice. ADSC, adipose-derived mesenchymal stem cells; EVs, extracellular vesicles; PD, Parkinson's disease; TH, tyrosine-hydroxylase.

## 2 | MATERIALS AND METHODS

### 2.1 | Animals

Female 8-week-old C57BL/6 mice were purchased from Orient Bio Inc. in Sunnam, Korea. The mice were kept in a pathogen-free environment with a 12 h light/dark cycle and unlimited access to food and water. All experiments involving live animals complied with the relevant laws and institutional guidelines of Sungkyunkwan University, and the Institutional Animal Care and Use Committee (IACUC) of Sungkyunkwan University approved all the experiments (SKKUIACUC2019-06-07-1, SKKUIACUC2023-02-74-1).

### 2.2 | Cell culture and conditioned medium collection

SH-SY5Y neuroblastoma cells and HEK293T cells were cultured in Dulbecco's Modified Eagle's Medium (DMEM) (Corning, #10-013-CV) supplemented with fetal bovine serum (Gibco, #12483020), and 1% penicillin-streptomycin (Capricorn, PS-B) at 37°C humidified air containing 5% CO<sub>2</sub>. Primary human ADSCs (age 38, female, 70E21-062) were purchased from Cefobio Inc. (Seoul, Korea) and cultured in DMEM supplemented with 10% fetal bovine serum and 1% penicillin/streptomycin at 37°C in humidified air containing 5% CO<sub>2</sub> to passage 6. Before replacing it with a conditioned medium, ADSCs were incubated to

reach 90% confluence. Then, the cells were washed with phosphate-buffered saline and the medium was replaced with serum-free DMEM for 24 h. The conditioned media was collected and then clarified via serial centrifugation (5 min, 300 x g, 20 min, 3000 x g at 4°C) to deplete cell debris and filtrated through a 0.22 µm membrane to remove the cell fragments. The resulting supernatant was carefully collected to obtain the final conditioned medium, which was then stored for the isolation of EVs.

### 2.3 | EVs isolation from conditioned medium

EVs were isolated from the conditioned medium using a method previously described (Jung et al., 2020). Briefly, EVs were purified from a 500 mL conditioned medium by a multi-filtration system based on tangential flow filtration (Minimate TFF System; Pall Corporation, Port Washington, NY, USA). The conditioned medium was subjected to filtration with a 300 kDa MWCO capsule (Minimate TFF Capsule; Pall Corporation, Port Washington, NY, USA). Continuous circulation was performed at a feed rate of 30~60 mL/min, and the filtrate rate was controlled around 4 mL/min to remove the contaminants below 300 kDa. Subsequently, two more TFF cycles were performed by adding 50 mL of PBS to wash residual contaminants in concentrated EV solution. Throughout the TFF process, the pressure was controlled not to exceed 1 bar at room temperature. EVs were obtained in a final volume of approximately 10 mL. EVs were stored in a freezer at -70°C until use.

### 2.4 | Surface modification of adipose-derived stem cell EVs

Dopa-EVs were prepared using an N-(3-Dimethylaminopropyl)-N'-ethylcarbodiimide/N-Hydroxysulfosuccinimide (EDC/Sulfo-NHS). The carboxyl group of the exosomal surface protein in 1 mL PBS (pH 6.5, 200 µg/mL) was activated with EDC (10 µL, 200 mM) and Sulfo-NHS (10 µL, 200 mM) for 30 min at room temperature. Dopamine (10 µL, 200 mM) was added to the solution and incubated for 6 h under gentle stirring at 4°C. Purification was carried out by using a 0.45 µm syringe filter and gravity flow columns (PD-10 Desalting columns; GE Healthcare, USA) in PBS (pH 7.4) to remove unreacted EDC/Sulfo-NHS and dopamine.

### 2.5 | EVs characterization

We isolated and characterized EVs following the instructions described in Minimal Information for Studies of Extracellular Vesicles 2023 (MISEV2023) provided by the *International Society for Extracellular Vesicles* (Welsh et al., 2024). To characterize the size distribution and concentration of EVs, nanoparticle tracking analysis (NTA) was performed using Nano Sight LM10 (Malvern Instruments, Malvern, UK) equipped with a 488 nm laser and syringe pump system. The parameters of NTA measurement were set as follows: Capture duration: 30 s, shutter speed: 30 ms, screen gain: 10, detection threshold: 5 and numbers of frame: 20~40 particles/frame. To observe EVs morphology, EVs suspension in PBS was loaded onto size 400-mesh, carbon-coated copper grids (Ted Pella Inc., Redding, CA). The grids were then washed with PBS, followed by staining with 2% uranyl acetate. The air-dried grids were visualized using transmission electron microscopy (TEM; JEOL-2100F, JEOL Ltd., Tokyo, Japan) at an accelerating voltage of 200 kV. To verify the successful modification of Dopa-EVs, BLI experiments were performed on a BLItz system (FortéBio, CA, USA). First, anti-dopamine antibody (50 µg/mL, 30 min, ab23969, Abcam) was immobilized on a AR2G biosensor (Sartorius, Goettingen, Germany). The sensors were then washed with the kinetics buffer (30 s). Functionalized sensors were reacted with ADSC-EVs and Dopa-EVs for the association steps ( $2 \times 10^{10}$  particles/mL, 120 s). After these steps, the sensors were immersed in the kinetics buffer for the dissociation steps (120 s). All sensorgrams were corrected for baseline drift by subtracting a control sensor exposed to running buffer only. For a competitive ligand binding assay, dopamine-conjugated BSA (40 µg/mL) was used. To quantify the protein concentration of EVs, a micro-bicinchoninic acid protein assay (Thermo Scientific, Rockford, IL, USA) was performed according to the manufacturer's instruction. All relevant data from the experiments were submitted to the EV-TRACK knowledgebase (EV-TRACK ID: EV230960) <https://evtrack.org/search.php> (Van Deun et al., 2017).

### 2.6 | ELISA

For the assessment of the concentration of dopamine on Dopa-EVs (20 µg/mL), ELISA plates were coated with a monoclonal antibody against dopamine (clone 5H1-A3) overnight at room temperature. Free binding sites were blocked with a blocking buffer for 2 h at room temperature. After washing the plates with 0.05% Tween 20 in PBS, EVs and standard samples were added to each well and incubated for 2 h at room temperature. Biotinylated anti-dopamine antibody was added to each well and incubated for 2 h, and then horseradish peroxidase-conjugated streptavidin was incubated for 20 min. After incubation, the plate was incubated with a substrate solution composed of a mixture of H<sub>2</sub>O<sub>2</sub> and tetramethylbenzidine for 20 min and then a stop

solution containing 2 N H<sub>2</sub>SO<sub>4</sub>. The plate was immediately read at 450 nm using a plate reader. The cut-off value (the limit of quantitation; LOQ) was determined based on the value specified in the ELISA kit instructions.

## 2.7 | $\alpha$ -synuclein preformed fibril preparation and activation

Previous research has described the preparation of  $\alpha$ -Syn PFF to induce PD in primary mouse neurons (Kam et al., 2018; Park et al., 2022). And 14 days after 5  $\mu$ g/mL  $\alpha$ -Syn PFF treatment showed 20%~30% neuronal death (Volpicelli-Daley et al., 2014). Briefly, 5 mg/mL  $\alpha$ -Syn PFF was diluted to 0.1 mg/mL with PBS and sonicated 4 times for 15 s (1 s pulse on/off) at 20% amplitude. On day 7 of neuronal differentiation, primary mouse neurons were treated with 1 or 5  $\mu$ g/mL of sonicated  $\alpha$ -Syn PFF for immunocytochemistry, immunoblot, or cell viability assays.

## 2.8 | Primary neuronal culture and treatment

Primary mouse neurons were prepared as previously described (Han et al., 2021; Park et al., 2021). Briefly, mouse pups at embryonic 17.5 day, derived from C57BL/6J background mice, were sacrificed, and whole brain tissues were collected. Subsequently, cortices were dissected from the harvested tissues. After removing meninges, tissues were transferred into cold PBS including 1% penicillin and streptomycin. Cortices were digested using 0.125% trypsin. Dissociated cells were neutralized by 10% FBS containing high glucose DMEM and followed by filtrating cells through 0.22  $\mu$ m pore-sized mesh. Cells were seeded onto Poly-D-lysine coated culture plates which coated the day before primary neuronal culture for overnight incubation. Primary mouse neurons were differentiated in Neurobasal medium (Gibco, #21103-049) supplemented with B-27 supplement (Gibco, #17504-044), and 1% penicillin-streptomycin at 37°C humidified air containing 5% CO<sub>2</sub>. Half of the neuronal culture medium was replaced with fresh medium every 3 days. On day 7 of differentiation, neurons were treated once with activated  $\alpha$ -Syn PFF and then maintained for an additional 14 days. 5  $\times$  10<sup>8</sup> particles/mL of ADSC-EVs or Dopa-EVs were added every 3 days after  $\alpha$ -Syn PFF treatment.

## 2.9 | Cell viability assay

The cell viability assay was performed according to the manufacturer's instructions using the Quanti-MAX WST-8 assay (Biomax, QM2500). Briefly, primary neurons were treated with 5  $\mu$ g/mL of sonicated  $\alpha$ -Syn PFF once on day 7, followed by Dopa-EVs treatment at a concentration of 1  $\times$  10<sup>8</sup> to 1  $\times$  10<sup>9</sup> particles/mL every 3 days thereafter. On day 21, 40  $\mu$ L of WST-8 assay solution was added, followed by a 3 h incubation. The absorbance was measured at 450 and 650 nm using a microplate reader.

## 2.10 | In vitro cellular uptake assay

The near-infrared fluorophore-labelled EVs were freshly prepared using Cy5.5-NHS ester (Lumiprobe, MD, USA). To monitor the cellular uptake of EVs, Cy5.5 mono NHS ester was chemically conjugated to amine groups on the surface of EVs. In brief, 200  $\mu$ g of EVs were suspended in PBS (pH 7.4) and mixed with a Cy5.5-NHS solution in DMSO. The reaction was conducted at 4°C overnight under continuous stirring. The reaction mixture was purified using gravity flow columns (PD-10 Desalting columns; GE Healthcare, USA) to remove unreacted free dyes. The fluorescence intensity of labelled ADSC-EVs and Dopa-EVs was measured to normalize the amount of EVs used in subsequent cellular uptake experiments. Thereafter, the labelled EVs were incubated with primary neuron cells with the seeding intensity of 2  $\times$  10<sup>4</sup> cells/cm<sup>2</sup> in a 24-well plate in the dark for 1, 3, 6, 24 h. For uptake assays with dopamine receptor blocking, SH-SY5Y cells were pre-incubated with dopamine receptor 1 (DIR) (ab20066, Abcam) antibody and D2R (AB5084P, Sigma) antibody (10  $\mu$ g/mL) for 3 h, or with a control rabbit IgG (GTX35035, GeneTex) antibody at the same concentration. After antibody incubation, cells were treated with Cy5.5-labelled EVs for 3 h in the dark. For the competition assay, cells were incubated with dopamine-containing medium (2 mg/mL in serum-free DMEM) for 2 h. Afterwards, the cells were exposed to Cy5.5-labelled -EVs (1  $\times$  10<sup>7</sup> particles/dish) for 3 h. The preparations were then fixed with 4% paraformaldehyde for 20 min, after that, the cell nucleus was stained with 6-diamidino-2-phenylindole (DAPI, Sigma, USA). EVs internalized by cells were visualized with a confocal microscope.

## 2.11 | 6-OHDA--induced PD mouse model

For injection of 6-OHDA into the medial-forebrain bundle, 8- to 10-week-old C57BL/6 male mice were deeply anaesthetized using a mixture of Zoletil (30 mg/kg) (Virbac) and Rompun (10 mg/kg) (Bayer) diluted at a 1:10 ratio with saline. They were then



positioned in a stereotaxic mouse frame. 6-OHDA (R&D Systems) was dissolved in 0.02% ascorbate (Sigma-Aldrich)/saline solution at a concentration of 5 mg/mL and used within 3 h. The injection was administered at a rate of 0.2  $\mu$ L/min into the medial forebrain bundle at the following coordinates (relative to the bregma): anterior–posterior (A/P) =  $-1.2$  mm, mediolateral (M/L) =  $-1.2$  mm, and dorsal–ventral (D/V) =  $-4.85$  mm (from the dura). After the injection, the syringe remained in place for an additional 5 min within the brain before being slowly withdrawn for a complete absorption of the solution. Control mice were injected with 0.02% ascorbic acid solution alone. To relieve mouse pain and improve survival rate after surgery, acetaminophen at a dose of 150 mg/kg was administered to mice twice a day for 3 days after injection of 6-OHDA. After discrimination of PD-induced mice using the pole-test, EVs were administered intravenously ( $5 \times 10^8$  particles/head) every 2 days for 5 weeks, starting 3 days after 6-OHDA injection.

## 2.12 | $\alpha$ -Syn PFF-induced PD mouse model

For intrastriatal injection of  $\alpha$ -Syn PFF, 3-month-old C57BL/6 male mice were deeply anesthetized. 5  $\mu$ g  $\alpha$ -Syn PFF was unilaterally injected into the striatum (2  $\mu$ L per hemisphere at 0.4  $\mu$ L/min) with the following coordinates: A/P =  $+0.2$  mm, mediolateral M/L =  $+2.0$  mm, D/V =  $+2.8$  mm from bregma. After the injection, the needle was maintained for an additional 10 min for complete absorption of the solution. To confirm the therapeutic effect of Dopa-EVs, EVs were administered intravenously ( $5 \times 10^8$  particles/head) twice a week for 5 months after 1 month of  $\alpha$ -Syn PFF injection. Behavioral tests were performed 6 months after the  $\alpha$ -Syn PFF injection. To observe in vivo biodistribution of EVs assay in PD mice, the assay was conducted 6 months after  $\alpha$ -Syn PFF injection.

## 2.13 | Motor function analysis

### 2.13.1 | Pole test

A wooden rod (75 cm long with a 10 mm diameter) wrapped with bandage gauze was used as the pole. Before the actual test, the mice were trained for a day and each training session consisted of three test trials. Mice were placed 10 cm apart from the top of the pole and faced upward. The total time to reach the base of the pole was measured. The test was finished by landing all 4 paws on the base. The maximum cutoff time to stop the test and recording was 120 s.

### 2.13.2 | Rotarod test

Mice were trained on a rotarod apparatus (Ugo-Basile, Italy) at 5 rpm for 300 s to walk onto the rotating rod. The test was conducted with a gradually accelerated speed from 5 to 40 rpm over a period of 300 s and measured the time until mice fell into the bottom. Also, the recording ended when each mouse just rotated without walking. Each animal was tested three times for 3 consecutive days and was taken to rest for at least 10 min between trials.

### 2.13.3 | Gait analysis

A 60 cm long, 10 cm wide runway was lined with white paper at the bottom. The paws of the mice were dipped in water-soluble non-toxic paint (forepaws purple, hind paws blue) and mice were allowed to run down the runway. The stride distance and the centre point of each paw were measured using ImageJ 1.48v software (NIH).

### 2.13.4 | Limb clasping analysis

Mice were suspended by their tail and the degree of hindlimb clasping was observed for 30 s. A score of 0 was given if no limb clasping and normal escape extension were observed. A score of 1 was assigned if one hindlimb exhibited incomplete splay, along with loss of mobility and the toes were splayed. A score of 2 was assigned if both hindlimbs exhibited partial splaying, accompanied by a loss of mobility and toes exhibited a normal splay. A score of 3 was assigned if both hindlimbs were fully clasped with curled toes and immobility (Miedel et al., 2017).

## 2.14 | In vivo biodistribution

To assess the biodistribution of the ADSC-EVs and Dopa-EVs, 6-OHDA-induced PD mice or  $\alpha$ -Syn PFF-induced PD mice were prepared as described above. 200  $\mu$ L of a solution containing Cy5.5-ADSC-EVs, Cy5.5-L-DOPA-EVs or Cy5.5-Dopa-EVs was injected via the tail vein of each mouse, and the time-dependent biodistribution was observed using an IVIS Lumina III In Vivo Imaging System (Caliper Life Sciences, MA, USA) with a 670 nm pulsed laser diode at the BIORP of Korea Basic Science Institute (KBSI). To observe the organ distribution, the major organs and brain were obtained and visualized using the IVIS Imaging System. All fluorescence images were obtained at wavelengths of 675 nm (excitation) and 730 nm (emission). The images were then quantified using the embedded software. In addition, the brains were excised, weighed, and subsequently homogenized with 1 mL of RIPA buffer by using a FastPrep-24 Sample Preparation System (MP Biomedicals, Solon, OH). The homogenate was then incubated at 4°C for 12 h. Next, 100  $\mu$ L of DMSO was added to the homogenates and the mixtures were incubated for 10 min. The tissue extracts were clarified by centrifugation at 15,000  $g$  for 15 min, and the fluorescence emission intensity levels of the supernatants were measured using a Nanodrop (Thermo Scientific, Rockford, IL, USA).

## 2.15 | Immunoblotting

Western blot analysis was performed as previously described (Seung Hyun et al., 2017). For analysis of the protein of interest, protein extracts were prepared using T-PER buffer (Thermo, #78510) containing 1x Halt protease cocktail and phosphatase inhibitors (Thermo, #78444). After 20 min cell lysis on ice using a T-PER extraction buffer mixture, cell lysate was collected and centrifuged at 16,000  $g$  for 30 min. Supernatants were collected as T-PER soluble fraction and pellets were prepared for T-PER insoluble fraction. To fractionate the T-PER insoluble fraction, pellets were washed with 200  $\mu$ L T-PER buffer mixture and removed supernatant additional centrifugation at the same condition. Washed pellets were lysed in urea-sodium dodecyl sulfate (SDS) buffer (8 M Urea, 4% SDS, T-per; 25 mM bicine, 150 mM sodium chloride; pH 7.6). Supernatants were collected as T-PER soluble fractions. Protein concentrations were measured using a BCA protein assay kit (Thermo). Proteins were separated by SDS polyacrylamide gel electrophoresis and transferred to polyvinylidene difluoride (PVDF) membranes. Membranes were blocked in 5% non-fat milk for 1 h at room temperature, and incubated overnight at 4°C with antibodies raised against Calnexin (AB2301, Sigma-Aldrich), TSG101 (sc-7964, Santa Cruz Biotechnology), CD9 (sc-13118, Santa Cruz Biotechnology),  $\beta$ -actin (A2228, AC-15, Sigma-Aldrich), CD63 (MX-49.129.5, Santa Cruz), tyrosine hydroxylase (2792, Cell Signaling Technology),  $\beta$ -actin (A5316, clone AC-15, Sigma), Parkin (ab77924, clone Prk8, abcam), LC3B (NB100-2220, Novus Biologicals), NRF2 phospho (Ser40) (2073-1, Epitomics),  $\alpha$ -synuclein (610787, clone 42/ $\alpha$ -Synuclein, BD biosciences),  $\alpha$ -synuclein (610787, clone 42/ $\alpha$ -Synuclein, BD biosciences), Beclin-1 (A11761, ABclonal), Tubulin  $\beta$ 3 (TUBB3) (MMS-435P, clone TUJ1, Biolegend), Akt (9272, Cell Signaling Technology), Phospho-Akt (Ser473) (9271, Cell Signaling Technology), Phospho-GSK-3 $\beta$  (Ser9) (5558, D85E12, Cell Signaling Technology), GSK-3 $\alpha/\beta$  (sc-7291, 0011-A, Santa Cruz Biotechnology), Phospho-p44/42 MAPK (Erk1/2) (Thr202/Tyr204) (4370, clone D13.14.4E, Cell Signaling Technology) and p44/42 MAPK (Erk1/2) (4696, clone L34F12, Cell Signaling Technology). Membranes were then washed and followed by incubating with peroxide-conjugated anti-mouse or antirabbit secondary antibodies (Millipore) for 1 h at room temperature. Protein bands were detected using ECL solution (Pierce). Densitometric quantification of western blot results was performed using ImageJ 1.48v (NIH).

## 2.16 | Immunohistochemistry

Immunohistochemistry was performed as previously described (Bahn et al., 2019). Briefly, after mice were perfused transcardially with 4% paraformaldehyde (PFA) in PBS, brains were removed and immersed in 4% PFA in PBS at 4°C overnight for fixation. Brains were then transferred to a sucrose solution to gradually dehydrate in 10%, 20%, and 30% sucrose solutions in PBS and stored at 4°C until cryosectioning for cryoprotection. Brain tissue was sectioned at a thickness of 30  $\mu$ m on a cryostat. Sections were blocked with 1% donkey serum (Biorad) to prevent non-specific binding of the antibodies. Sections were then incubated with primary antibodies against tyrosine hydroxylase (22941, clone LNCl, Immunostar) or GFAP (Z0334, Dako) at 4°C overnight. The brain sections were then washed with PBS and incubated for 1 h in the presence of anti-mouse IgG labelled with Alexa Fluor-594 (Invitrogen) and anti-rabbit IgG labelled with Alexa Fluor-488 (Invitrogen) to visualize the primary antibodies. Nuclei of immune-labelled specimens were stained with DAPI (Molecular probes, Karlsruhe). Images were acquired using a confocal microscope LSM700 (Carl Zeiss). The area of TH-positive cells in the SNpc region was analyzed using ImageJ 1.54 software.

## 2.17 | Quantitative real time-PCR

Total RNA extraction and qPCR were performed as previously described (Kim et al., 2024; Lee et al., 2021). Total RNA was isolated from HEK293T and SH-SY5Y cells using RNAiso Plus (Takara Bio) following the manufacturer's instructions. The extracted RNA was then reverse-transcribed into complementary DNA using the PrimeScript RT Reagent Kit (Takara Bio). Quantitative real-time PCR was carried out with TB Green Premix Ex Taq (Takara Bio). The primer sequences used for qPCR are provided in Table S1 with actin serving as the housekeeping gene.

## 2.18 | Statistical analysis

All experimental data were represented as mean  $\pm$  standard deviation (SD). One-way analysis of variance with *Tukey's post hoc* test was performed using GraphPad Prism 8 software (GraphPad, San Diego, CA, USA).  $p \leq 0.05$  was considered statistically significant.

# 3 | RESULTS

## 3.1 | Dopamine functionalization of ADSC-EVs via a two-step coupling

Human ADSCs were cultured, and EVs were isolated from their conditioned medium using a tangential flow filtration system. Dopamine was subsequently conjugated onto ADSC-EVs using EDC/Sulfo-NHS reaction (Figure 2a) (Suleiman et al., 2020; Wang et al., 2023). For this conjugation, the carboxyl groups on the proteins of the outer surface of ADSC-EVs or phosphatidylserine were activated by EDC/Sulfo-NHS to form a Sulfo-NHS ester intermediate (Wang et al., 2023). This intermediate then reacted with the primary amine of dopamine, creating a cross-linked amide bond. This efficient and versatile two-step reaction enabled the functionalization of dopamine onto the surface of ADSC-EVs without necessitating a linker (Grabarek & Gergely, 1990).

Western blot analysis was employed to assess the enrichment of EVs markers post-dopamine engineering. Results indicated that markers such as CD9, CD63, and TSG101 were significantly enriched in both ADSC-EVs and Dopa-EVs, whereas Calnexin was only detected in the cell lysates (Figure 2b). TEM images revealed that Dopa-EVs retained a round shape with a bilayer structure and were well-dispersed (Figure 2c). Also, The size distribution of both Dopa-EVs and unmodified EVs demonstrated similar diameters (Figure 2d), with the mean size of Dopa-EVs being  $182.2 \pm 60.8$  nm, not significantly different from that of ADSC-EVs ( $183.1 \pm 55.3$  nm) (Figure 2e). L-DOPA, a dopamine precursor, was also engineered onto EVs surface (L-DOPA-EVs) to explore BBB crossing via L-type transporter-1 (LAT-1) (Hiroshi et al., 2002; Montaser et al., 2020; Puris et al., 2020). TEM and NTA results indicated that L-DOPA-EVs remained well dispersed and retained small EV size post-modification (Figure S1A,B). However, the zeta potential of L-DOPA-EVs shifted to 0 mV, implying a loss of colloidal stability (Figure S1C) (Midekessa et al., 2020). These results collectively demonstrate that dopamine conjugation does not alter the fundamental physical and biological properties of the EVs.

## 3.2 | Dopa-EVs target dopaminergic neurons through dopamine receptors

To investigate whether Dopa-EVs target dopaminergic neurons through dopamine receptors, we quantified dopamine concentration in Dopa-EVs using ELISA. The dopamine concentration in Dopa-EVs was found to be approximately  $646.25 \pm 18.5$  pg/mL, while in unmodified ADSC-EVs it was below the quantitation limit of the assay (Figure 3a). Bio-layer interferometry (BLI) was utilized to examine the binding affinity of Dopa-EVs with dopamine antibodies (Kim et al., 2022; Lim et al., 2021). BLI signals, indicating specific interactions with the dopamine antibodies immobilized on a AR2G biosensor, were significantly enhanced in Dopa-EVs compared to ADSC-EVs (Figure 3b,c). Interestingly, this interaction was abolished by pre-treatment with dopamine-conjugated BSA (Dopa-BSA), suggesting successful functionalization on the surface of Dopa-EVs and functional interaction with dopamine receptors.

Moreover, we evaluated the behavior of Dopa-EVs in cellular systems by conducting cellular uptake in SH-SY5Y cells and primary neurons their receptor-mediated endocytosis. We confirmed that, compared to HEK293T cells, SH-SY5Y cells exhibited a higher expression of D2R than D1R (Figure S2A,B). The quantitation by confocal microscopy reveals a significant uptake of Dopa-EVs (1.36-fold higher uptake at 1 h time point, 1.53-fold higher uptake at 3 h time point) compared to ADSC-EVs in primary neurons (Figure 3d,e). The fluorescence intensity in both Dopa-EVs and ADSC-EVs had reached a plateau and appeared similar at 24 h (Figure S3A,B). This suggests that Dopa-EVs were taken up by cells via efficient mechanisms compared to ADSC-EVs. Enhanced intracellular uptake of Dopa-EVs via receptor-mediated internalization was further evident from a blocking assay,



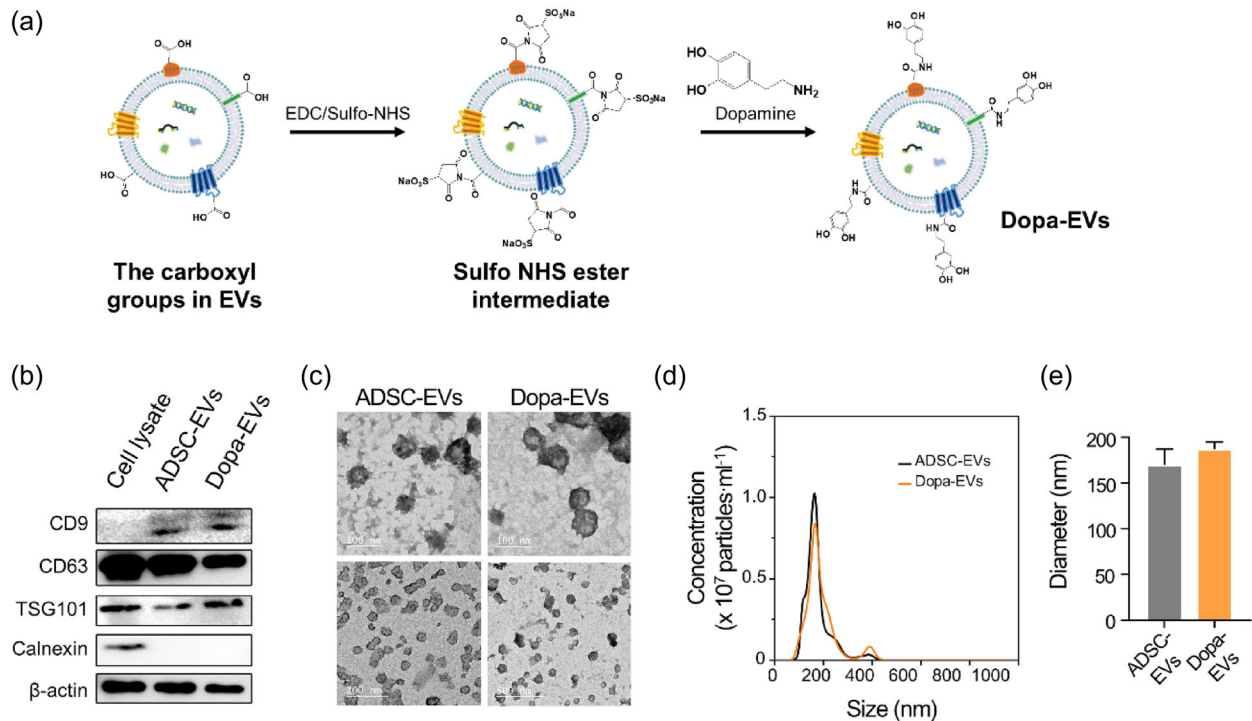


**FIGURE 2** Characterization of EVs. (a) Schematic diagram of conjugating dopamine to carboxyl groups of ADSC-EVs by a two-step coupling reaction. (b) Representative western blot analysis of cell lysates, ADSC-EVs, and Dopa-EVs. (c) TEM images of ADSC-EVs and Dopa-EVs. (d) Size distribution and (e) average diameter of ADSC-EVs and Dopa-EVs measured by NTA. Data represent mean  $\pm$  SD. ADSC, adipose-derived mesenchymal stem cells; EVs, extracellular vesicles; NTA, nanoparticle tracking analysis.

substantiating the observation from the uptake study (Figure 3f). Dopa-EVs exhibited higher cellular uptake in both untreated and IgG-treated SH-SY5Y cells, while the uptake of Dopa-EVs was reduced to levels comparable to that of ADSC-EVs when D1R or D2R antibodies were used to block the receptors (Figure 3g). Pre-treatment with dopamine also impeded the uptake of Dopa-EVs in both primary neurons and SH-SY5Y cells (Figure S2C,D), consistent with receptor competition blocking Dopa-EV internalization. These findings indicate that dopamine conjugation enhances in vitro cellular uptake of Dopa-EVs, mediated via dopamine receptors.

### 3.3 | In vivo delivery of Dopa-EVs to the brain

To examine the in vivo brain distribution of Dopa-EVs in a PD model, we intravenously administered Free-dye, Cy5.5-labelled ADSC-EVs and Dopa-EVs in 6-OHDA induced PD mice. Notably, the Dopa-EV-injected group exhibited prolonged and stronger intensity in the brain tissue compared to the ADSC-EVs-injected group over time (Figure 4a,b). The brain accumulation of Dopa-EVs was also compared to that of ADSC-EVs and L-DOPA-EVs in vivo in  $\alpha$ -Syn PFF-injected mice (Figure S4A).  $\alpha$ -Syn PFF were injected into the striatum of 3-month-old C57/BL6 mice (Figure S5A). Six months post  $\alpha$ -Syn PFF-striatal injection, motor dysfunction ensued, and  $\alpha$ -synuclein ( $\alpha$ -Syn) aggregation was observed in the insoluble fraction of the striatum in  $\alpha$ -Syn PFF-injected mice (Figure S5B–D). As expected, Dopa-EVs showed higher brain accumulation over time compared to other EVs (Figure 4b, Figure S4B). Ex vivo imaging and quantification of major organs were performed 12 h post-administration of each EV type in  $\alpha$ -Syn PFF-injected mice (Figure 4c,d). Of note, these results showed that the fluorescence of the brain in Dopa-EVs treated group was even stronger than those in Free dye or ADSC-EVs treated group. Although the liver remained the primary site of EV accumulation, the total quantity of the fluorescence in the brain calculated demonstrated that Dopa-EVs gained enhanced brain retention. Additionally, ex vivo imaging and brain homogenates analysis were carried out to depict the brain loads of Cy5.5. The fluorescence intensity and relative Cy5.5 concentration of Dopa-EVs in the brain were 1.38-fold and 1.75-fold higher, respectively, than those of ADSC-EVs (Figure 4e–g). These results suggest the successful targeting of dopaminergic neurons in the brain in vivo by dopamine-engineered EVs.

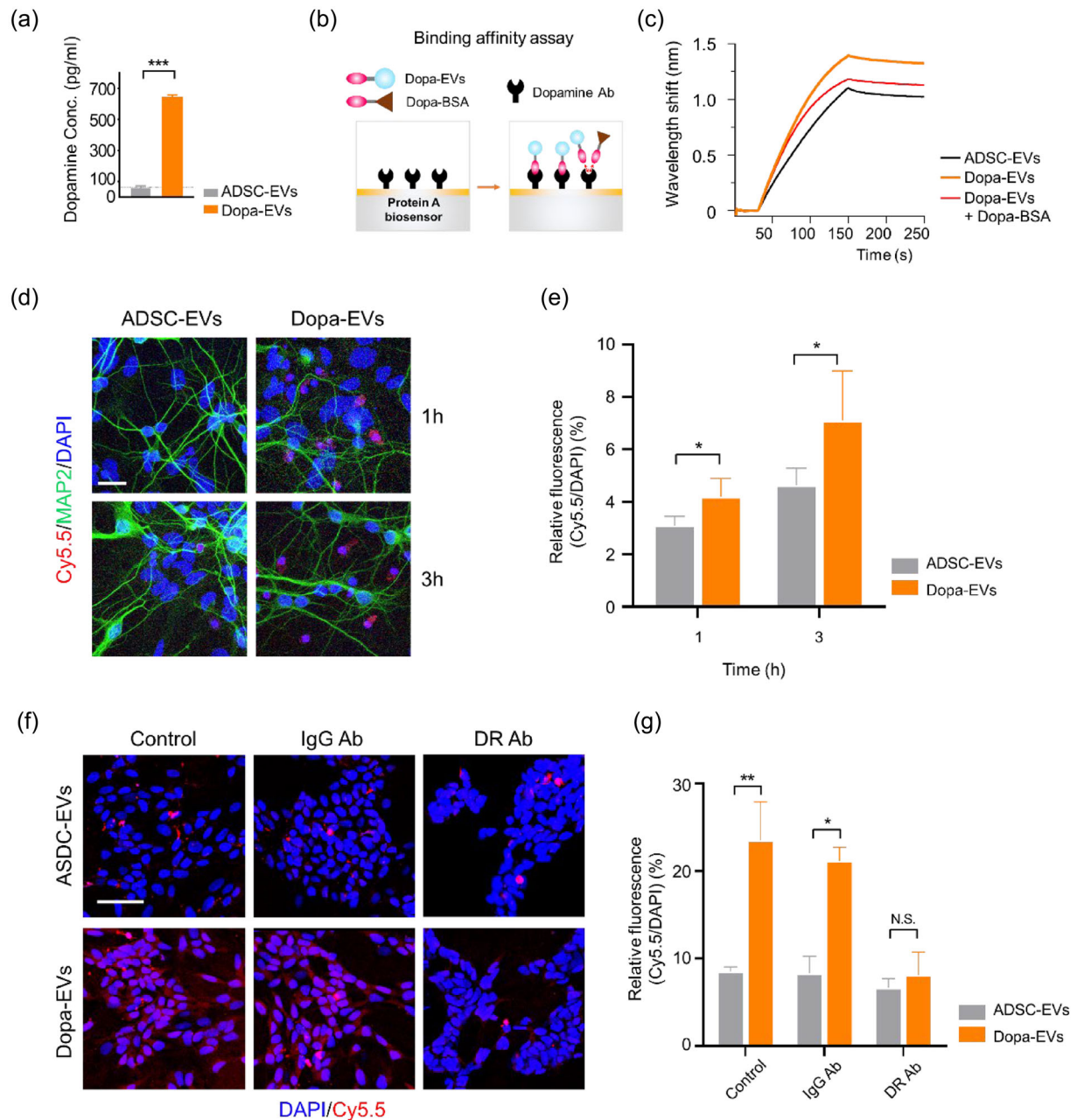


**FIGURE 3** Neuronal delivery of Dopa-EVs via dopamine receptors in vitro (a) Quantification of dopamine concentration in EVs using ELISA. The dotted line indicates the LOQ. (b) Schematic illustration of the binding affinity assay for Dopa-EVs using biolayer interferometry with dopamine antibody. (c) Binding kinetics of ADSC-EVs, Dopa-EVs, and Dopa-EVs with dopamine-conjugated BSA (Dopa-BSA) on dopamine antibody derivatized biosensors. Cellular uptake of Cy5.5-labelled ADSC-EVs or Dopa-EVs in primary mouse neurons at 1 and 3 h (d), with corresponding fluorescence quantification (e). Scale bar, 20  $\mu$ m. Cellular uptake of Cy5.5-labelled ADSC-EVs or Dopa-EVs in SH-SY5Y neuroblastoma cells pre-incubated with a nonspecific isotype control (IgG Ab) or monoclonal antibodies against D1R and D2R (DR Ab) (f), with corresponding fluorescence quantification (g). Scale bar, 50  $\mu$ m. Unpaired Student's *t*-test. \**p* < 0.05, \*\**p* < 0.01, and \*\*\**p* < 0.001. Data represent mean  $\pm$  SD. ADSC, adipose-derived mesenchymal stem cells; EVs, extracellular vesicles; LOQ, limit of quantitation.

### 3.4 | Amelioration of dopaminergic neuronal degeneration by Dopa-EVs in vivo PD model

To validate the therapeutic efficacy of Dopa-EVs in a PD mouse model, we utilized the 6-OHDA-induced PD model. Three days post 6-OHDA medial-forebrain injection, mice exhibited irregular gait and motor dysfunction (Figure S6A-F), coupled with significant dopaminergic neurodegeneration in the ipsilateral region of the striatum (Figure S6G). After segregating non-induced mice, Dopa-EVs were intravenously administered daily for 7 days, followed by motor function assessment (Figure 5a,b). Remarkably, Dopa-EVs significantly mitigated 6-OHDA-induced motor dysfunctions in both the pole-test and rotarod test (Figure 5c,d)

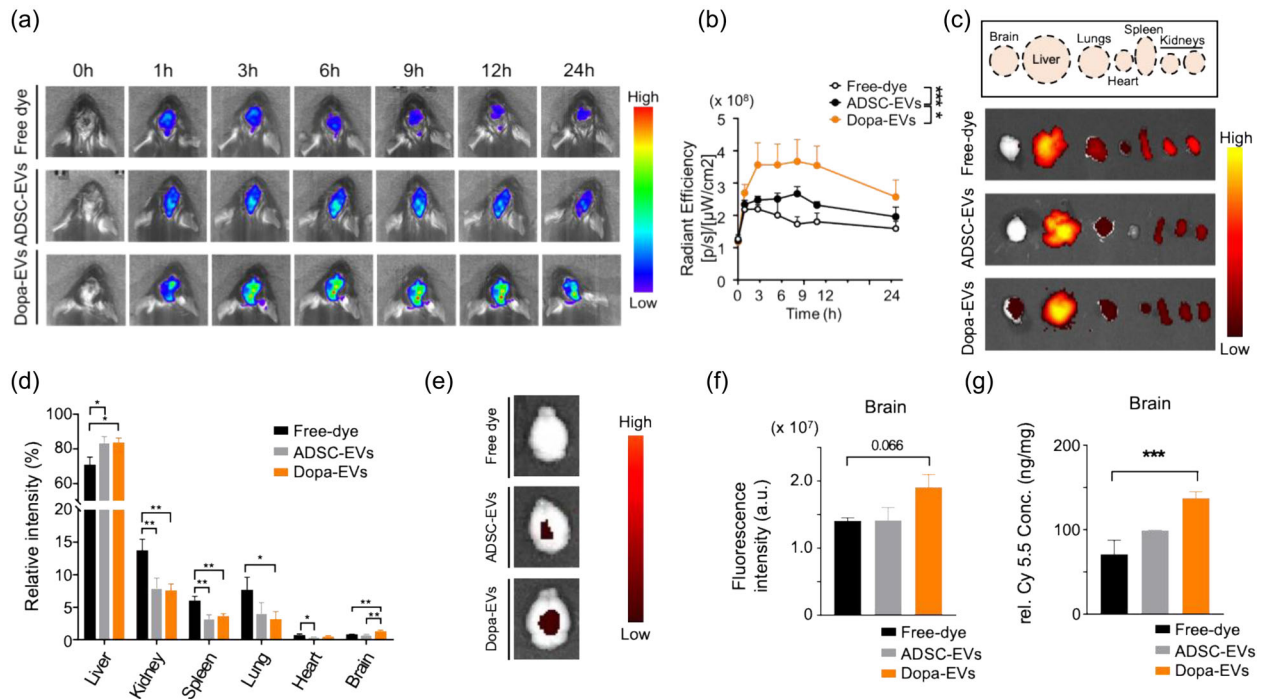


**FIGURE 4** Brain accumulation of Dopa-EVs in PD mice (a) Representative fluorescence images of biodistribution of Free dye, Cy5.5-labelled ADSC-EVs, and Dopa-EVs in 6-OHDA-induced PD mice as a function of time. (b) Quantification of in vivo fluorescence intensity of brain as a function of time ( $n = 4$ ). (c) Representative ex vivo fluorescence images of major organs in  $\alpha$ -Syn PFF-induced PD mice ( $n = 3$ ). (d) Quantification of ex vivo fluorescence intensity of major organs. (e) Representative ex vivo fluorescence images of brains ( $n = 3$ ). (f) Quantification of fluorescence intensity of brains (g) Quantification of fluorescence of brain homogenates. Data in (b) and (d) are analyzed by two-way ANOVA and data in (f) and (g) analyzed by unpaired Student's  $t$ -test. \* $p < 0.05$ , \*\* $p < 0.01$ , and \*\*\* $p < 0.001$ . Data represent mean  $\pm$  SEM.  $\alpha$ -Syn PFF,  $\alpha$ -synuclein preformed fibril; ADSC, adipose-derived mesenchymal stem cells; EVs, extracellular vesicles; PD, Parkinson's disease.

and improved gait deficit and stride length (Figure 5e,f). Corresponding with these motor function tests, immunohistochemical analysis revealed that Dopa-EV administration preserved TH-positive area in the ipsilateral region of striatum (Figure 5g,h) and SNpc (Figure 5i), compared to the contralateral region. Western blot analysis corroborated these findings, showing that Dopa-EVs treatment restored TH protein levels in the ipsilateral region, accompanied by upregulation of LC3-II, an autophagy marker (Figure 5j-l). In addition, the anti-Parkinson's effect of Dopa-EVs were investigated in an  $\alpha$ -Syn PFF-induced PD mouse model. Here, EVs were administered intravenously twice weekly for 5 months, commencing 1-month post- $\alpha$ -Syn PFF injection (Figure S7A). At 6 months post-injection, both EV groups demonstrated marginal improvement in motor dysfunction in the rotarod test (Figure S7B). Given that cerebellar ataxia is induced by neurodegeneration and aging (Miedel et al., 2017), limb clasp was measured to assess cerebellar ataxia (Figure S7C), revealing that the Dopa-EVs-injected group exhibited significant amelioration of cerebellar ataxia (Figure S7D). These results collectively suggest that Dopa-EVs can restore dopaminergic degeneration and ameliorate motor dysfunction caused by pathological  $\alpha$ -Syn and 6-OHDA.

### 3.5 | Dopa-EVs induce autophagy in PD in vitro

To explore the therapeutic effects and underlying mechanisms of Dopa-EVs on PD in vitro, we first assessed cell viability in the 6-OHDA-induced PD model. Treatment with Dopa-EVs effectively mitigated 6-OHDA-induced neurodegeneration in primary neurons (Figure 6a). Additionally, Dopa-EVs upregulated normal TH expression (Figure 6b,c). Dopa-EVs upregulated total Beclin-1 and LC3-II levels in a concentration-dependent manner, paralleling the effects of ADSC-EVs (Figure 6b,c). Furthermore, the reduced LC3 induction in 6-OHDA-treated dopaminergic neurons was restored in neurons treated with Dopa-EVs (Figure 6d,e).

We also verified the anti-Parkinson's effects of Dopa-EVs against toxic  $\alpha$ -Syn in primary neurons (Figure 7a). Dopa-EVs displayed a concentration-dependent neuroprotective effect against toxic  $\alpha$ -Syn (Figure 7b) and upregulated levels of LC3-II and Parkin, central to mitophagy (Figure 7c). Also, both Dopa-EVs and ADSC-EVs attenuated  $\alpha$ -Syn aggregation and phosphorylation from 12 days after  $\alpha$ -Syn PFF treatment (Figure 7d,e). To determine if the neuroprotective effects of Dopa-EVs were mediated by the delivery of intact EVs, we evaluated the anti-Parkinson's effect of post-sonication-induced membrane disruption.



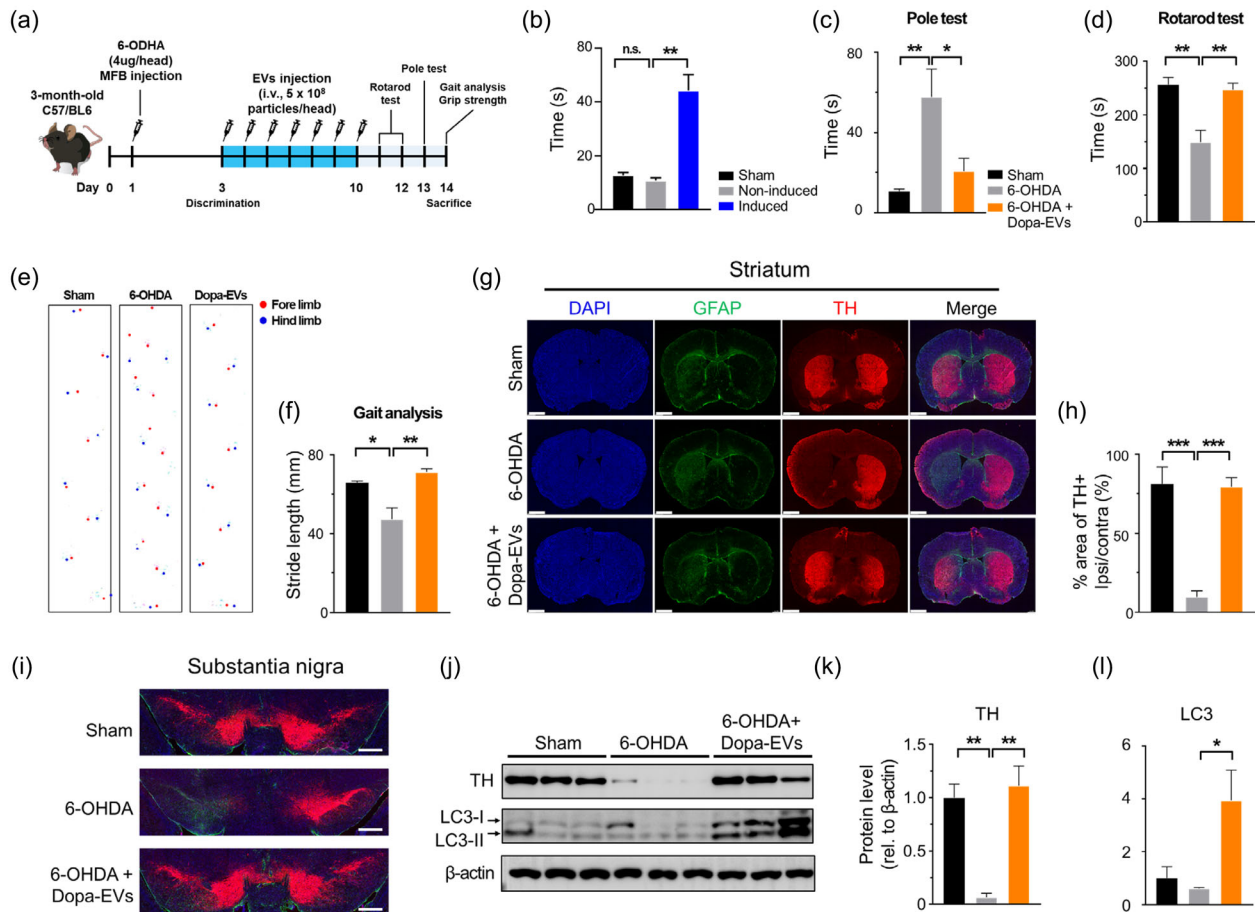


**FIGURE 5** Improvement of dopaminergic nigrostriatal degeneration by Dopa-EVs in vivo PD mice (a) Schematic illustration of experimental design. (b) Pole test for discriminating PD induced mice 3 days after unilateral injection of 6-OHDA. (c–f) Behavioural assessment of Sham ( $n = 5$ ), Vehicle (6-OHDA,  $n = 11$ ) and Dopa-EVs (6-OHDA + Dopa-EVs,  $n = 9$ ) injected mice after 7 consecutive days of intravenous injection. Representative double immunostaining for GFAP (green) and tyrosine hydroxylase (TH, red) in the (g) striatum and (i) substantia nigra. Scale bar, 500 μm. (h) Quantification of the relative TH-immunoreactive area in the ipsilateral region of the striatum compared to the contralateral region ( $n = 4$ ). (j) Western blot analysis of TH and LC3 in the ipsilateral region of mice striatum. Quantification of TH (k) and total LC3-II (li) protein expression levels in the ipsilateral region of mice striatum ( $n = 3$ ). One-way ANOVA followed by Tukey's post hoc test. \* $p < 0.05$ , \*\* $p < 0.01$ , and \*\*\* $p < 0.001$ . Data represent mean  $\pm$  SEM. ADSC, adipose-derived mesenchymal stem cells; EVs, extracellular vesicles; TH, tyrosine-hydroxylase.

tion of Dopa-EVs (Figure 7f). Intriguingly, disrupting the membrane integrity of Dopa-EVs abolished these anti-Parkinson's effects (Figure 7g), indicating that the therapeutic efficacy of Dopa-EVs is mediated by their intravascular contents. Additionally, to verify whether the effects of Dopa-EVs are due to the agonistic effect of dopamine present on the EV surface, we treated SH-SY5Y cells with EVs and dopamine to observe if the downstream signaling pathways of dopamine receptors were activated. Based on ELISA results (Figure 3a), the concentration of dopamine present in  $4 \times 10^9$  particles/mL of Dopa-EVs was estimated to be approximately 8.4 nM. When SH-SY5Y cells were treated with ADSC-EVs, Dopa-EVs, and 0.3 μM dopamine for 2 h, AKT, GSK, and ERK were not activated; however, these pathways were activated at 10,000- and 100,000-fold (30 and 300 μM) higher dopamine concentrations (Figure S8A). Furthermore, after 24 h of treatment, toxicity due to dopamine oxidation was not observed in 0.3 μM dopamine or Dopa-EVs (Figure S8B) (Burbulla et al., 2017; Choi et al., 2010). In summary, Dopa-EVs protect dopaminergic neurons from 6-OHDA and toxic α-Syn and mitigate α-Syn aggregation and phosphorylation by inducing autophagy through the delivery of intact EVs, without causing dopamine oxidation toxicity or activating dopamine signaling.

## 4 | DISCUSSION

G-protein coupled receptors (GPCRs) are integral membrane proteins that play a crucial role in transmitting extracellular signals into cells, with approximately 800 GPCR genes identified in humans (Congreve et al., 2020). D2R, one of the GPCR family, is predominantly localized in both post- and pre-synaptic regions in the VTA and SNpc. Notably, presynaptic D2R functions as an autoreceptor, regulating dopamine release and transmission in dopaminergic neurons (Ford, 2014; Yin et al., 2020; Zhuang

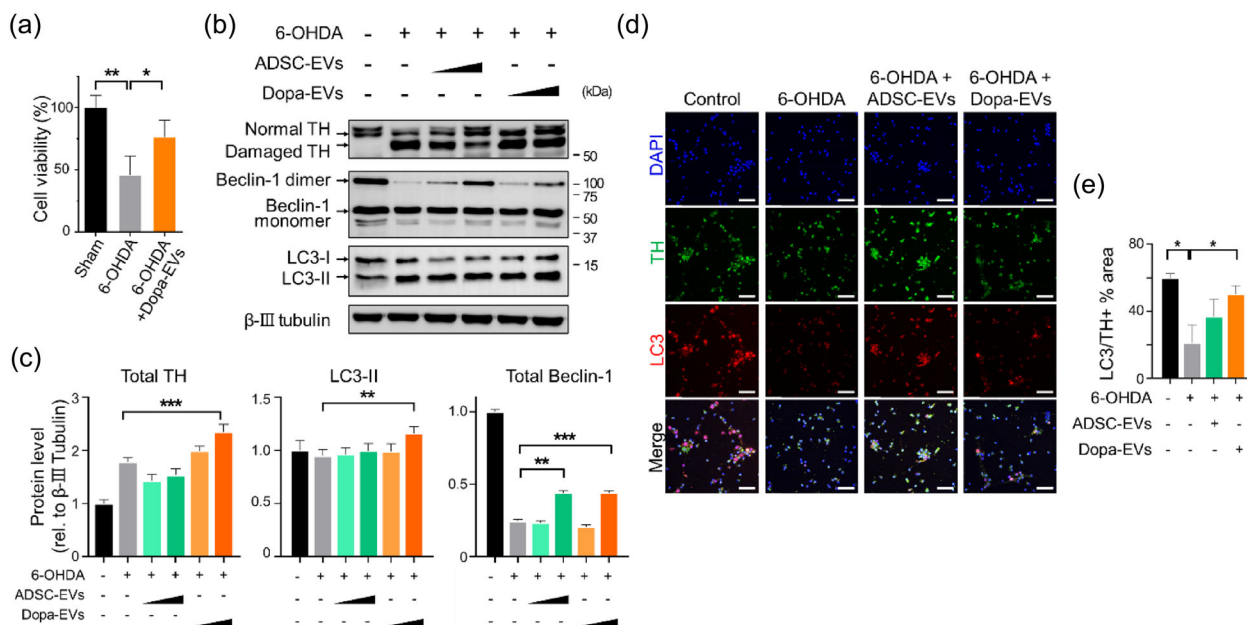


**FIGURE 6** Neuroprotective effect of Dopa-EVs on 6-OHDA in vitro via autophagy induction (a) Cell viability analysis using WST-8 in primary mouse neuron. (b–c) Representative western blot analysis and quantification results of the expression levels of TH, Beclin-1 and LC3-II in primary neurons treated as indicated. (d) Representative double immunostaining for TH (green) and LC3 (red) in the primary neurons. Scale bar, 500  $\mu$ m. (e) Quantification of the relative LC3 expression in TH+ area in primary neurons treated as indicated. One-way ANOVA followed by Tukey's post hoc test.  $n = 4$ , \* $p < 0.05$ , \*\* $p < 0.01$ , and \*\*\* $p < 0.001$ . Data represent mean  $\pm$  SD. TH, tyrosine-hydroxylase.

et al., 2021). Several amino acids are highly conserved in dopamine receptors across species, aspartate residue at position 114 has been identified as a critical site for binding dopamine's amine group, while serine residues at positions 195/197 enhance affinity by interacting with dopamine's catechol group. (Burns et al., 2019; Kalani et al., 2004; Zhuang et al., 2021) Recent cryo-electron microscopy (cryo-EM) studies extend the understanding of the interaction between dopamine receptors and various agonists and antagonists (Yin et al., 2020; Zhuang et al., 2021). Intriguingly, structural analyses imply that modifications to the amine group of dopamine exhibit greater flexibility than those made to the catechol group (Zhuang et al., 2021). This insight suggests that modifying the amine group of dopamine, rather than the catechol group, may better preserve the interaction between dopamine and its receptor, potentially allowing NPs or Dopa-EVs to more effectively target dopamine receptors in the dopaminergic neurons (Liu et al., 2021; Zhang et al., 2015). This modification decreases dopamine autooxidation and reduces neuronal death (Burbulla et al., 2017; Kim et al., 2024; Zhang et al., 2015).

In this study, we initially developed Dopa-EVs that display dopamine on the surface of ADSC-EVs using the EDC/Sulfo-NHS coupling reaction, which significantly enhances brain delivery by selectively targeting dopaminergic neurons in PD models. Historically, the efficient delivery of EVs to the brain for treating neurodegenerative diseases has presented considerable challenges (Choi et al., 2022). To address constraints, notable attempts included the transplantation of EVs secreting cells, targeting the acetylcholine receptor by overexpressing the Rabies virus glycoprotein for catalase-encoded mRNA delivery in PD (Kojima et al., 2018), the brain delivery of a glucose-presenting nanocarrier via glucose transporter-1 (GLUT-1) under fasting condition (Anraku et al., 2017), and the utilization of transferrin-enriched blood EVs for dopamine delivery across the BBB via receptor-mediated transcytosis (Qu et al., 2018). Our approach, utilizing a straightforward two-step coupling reaction, represents a significant advancement by enabling the rapid functionalization of pre-isolated EVs with dopamine while preserving their biological effects and physical characteristics. We clearly demonstrated that Dopa-EVs enhanced neuronal uptake via dopamine receptors, and this uptake was blocked by D1R and D2R antibodies, as well as dopamine-conjugated BSA in both of SH-SY5Y cells and primary mouse neurons. Remarkably, Dopa-EVs accumulated more in the brains of 6-OHDA and  $\alpha$ -Syn PFF-induced PD mice, resulting in significant improvements in motor dysfunction and dopaminergic neuronal degeneration in vivo. Collectively, as promising PD-modifying agents, Dopa-EVs specifically target dopaminergic neurons and mitigate PD through dopamine receptor-mediated endocytosis.

Dopamine, as an endogenous neurotransmitter in our body, can act as a double-edged sword. It stimulates receptors to either activate or inhibit downstream signaling pathways. However, an excessive amount of dopamine can undergo oxidation to oxidopamine, forming radicals that induce neuronal degeneration (Burbulla et al., 2017; Zhang et al., 2015). In our study, we observed that Dopa-EVs ameliorated cell death caused by 6-OHDA or toxic  $\alpha$ -Syn without any neuronal toxicity. Furthermore, these effects were abolished when the membrane of Dopa-EVs was disrupted. These results imply that the neuroprotective effect of Dopa-



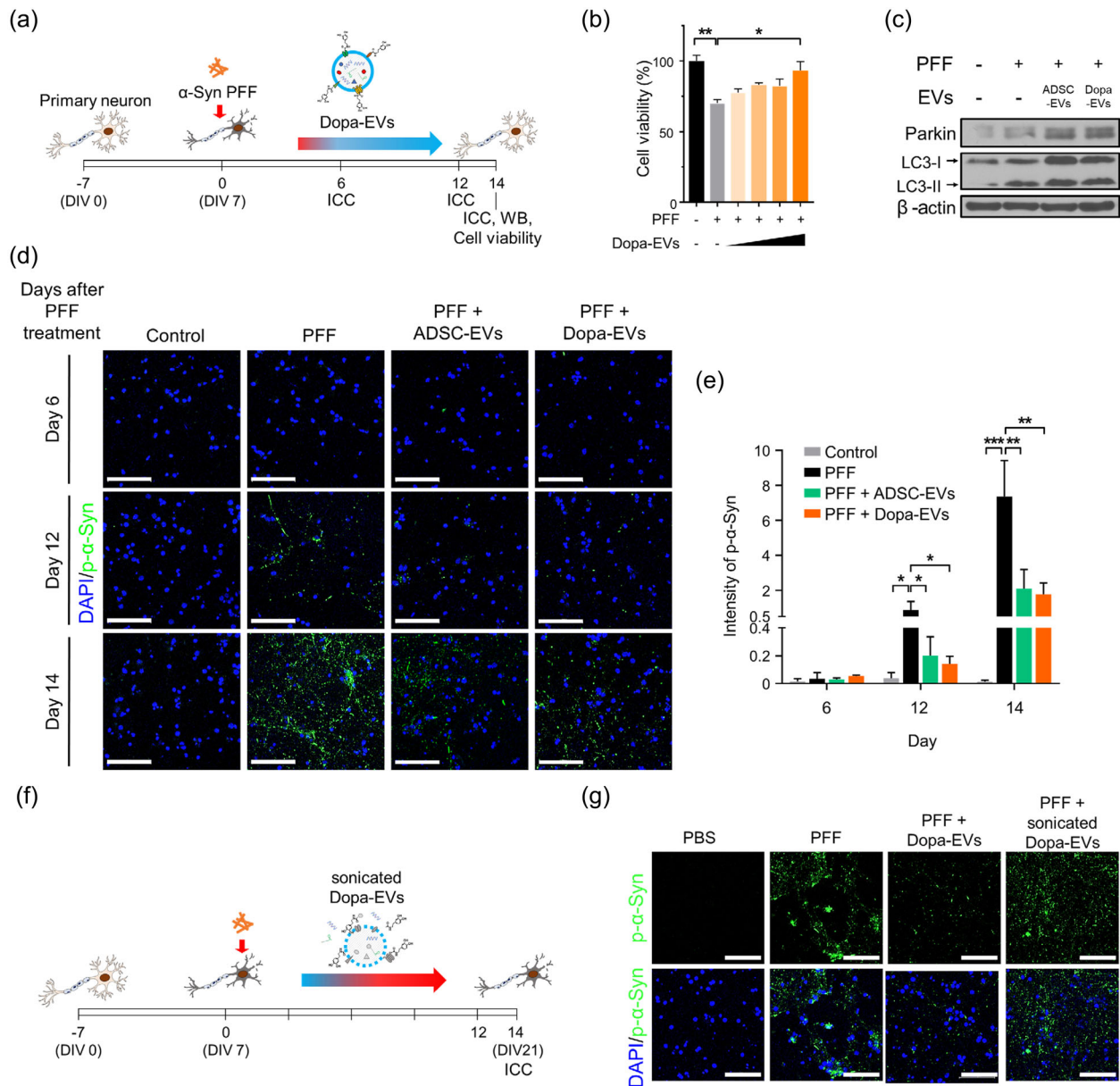


**FIGURE 7** Therapeutic effect of Dopa-EVs on  $\alpha$ -Syn PFF in vitro via autophagy induction. (a) Schematic diagram illustrating the treatment of Dopa-EVs in primary mouse neurons induced with  $\alpha$ -Syn PFF. (b) Amelioration of  $\alpha$ -Syn PFF-induced neuronal death in primary mouse neurons treated with Dopa-EVs, as determined by the WST-8 cell viability assay. (c) Representative Western blot analysis showing the expression levels of Parkin and LC3 in primary neurons treated as indicated. (d) Inhibition of  $\alpha$ -Syn PFF-induced propagation and phosphorylation of  $\alpha$ -Syn (green) by ADSC-EVs and Dopa-EVs in primary neurons. Scale bar: 100  $\mu$ m. (e) Quantitative analysis of the intensity of p- $\alpha$ -Syn over time ( $n = 3$ ). (f) Schematic diagram showing the treatment of Dopa-EVs or sonicated Dopa-EVs in  $\alpha$ -Syn PFF-induced primary mouse neurons. (g) Representative phospho- $\alpha$ -Syn (Ser129) immunostaining (green) in the Dopa-EVs or sonicated Dopa-EVs treated  $\alpha$ -Syn PFF-induced primary mouse neurons. Scale bar, 100  $\mu$ m. One-way ANOVA followed by Tukey's post hoc test.  $n = 4$ ,  $*p < 0.05$ , and  $**p < 0.01$ . Data represent mean  $\pm$  SD.  $\alpha$ -Syn PFF,  $\alpha$ -synuclein preformed fibril; ADSC, adipose-derived mesenchymal stem cells; EVs, extracellular vesicles.

EVs is achieved through EV delivery. Supporting this conclusion, treatment with Dopa-EVs and an equivalent concentration of dopamine present on the Dopa-EVs was insufficient to activate the downstream pathways of dopamine receptors.

Small EVs are promising vehicles due to their homing effect, high biocompatibility, and low immunogenicity. They can encapsulate a wide range of proteins and nucleic acids, allowing them to regulate endogenous targets within recipient cells (Han et al., 2024). As a major source of circulating miRNAs, ADSC-EVs carry diverse miRNAs that mitigate pathological conditions in osteoarthritis and frailty (Lee et al., 2021; Thomou et al., 2017). Our results indicate that the neuronal delivery of Dopa-EVs ameliorated dopaminergic neurodegeneration in both toxic  $\alpha$ -Syn and 6-OHDA-induced PD models, both in vitro and in vivo. This improvement is linked to the induction of autophagy, which is crucial for removing damaged organelles and abnormal protein

aggregates implicated in  $\alpha$ -Syn propagation and neuronal toxicity in PD (Choi et al., 2020; Minakaki et al., 2018; Nixon, 2013; Stavoe & Holzbaur, 2019; Tu et al., 2021). Several miRNAs have been reported to potentially upregulate autophagy (Ma et al., 2023), and ADSC-EVs carrying let-7a-5p in MSC-EVs have been shown to induce autophagy in AD (Lin et al., 2022). Numerous studies have reported that ADSC-EVs are promising drug candidates for various neurodegenerative diseases, such as ALS, AD, HD, and aging (Lee et al., 2018; Lee et al., 2016; Lee et al., 2016; Sanz-Ros et al., 2022). Specifically, ADSC-EVs facilitate the removal of amyloidogenic protein via activation of the cAMP Response Element-Binding Protein (CREB) signalling pathway (Hu et al., 2022; Lee et al., 2018; Lee et al., 2016), and CREB activation is known to induce autophagy, ameliorating Alzheimer's disease (Wang et al., 2021). In our study, Dopa-EVs significantly upregulated Beclin-1, Parkin, and LC3B levels, and rescued tyrosine hydroxylase, a marker of dopaminergic neurons, in both in vitro and in vivo models. However, the precise mechanisms by which ADSC-EVs and their internal molecules regulate autophagy in PD remain to be elucidated.

In summary, our findings indicate that dopamine conjugation onto the surface of EVs effectively targets dopaminergic neurons in the PD brain. The discovery paves the way for the use of Dopa-EVs as novel and selective disease-modifying agents for treating PD, utilizing autophagy induction as a therapeutic mechanism. This approach holds promise for modulating PD pathologies in diverse PD models, underscoring the potential of Dopa-EVs in the landscape of neurodegenerative disease treatment.

## AUTHOR CONTRIBUTIONS

Dong-Gyu Jo and Jae Hyung Park conceived the study. Dong-Gyu Jo, Jae Hyung Park, Jae Hoon Sul and Sol Shin designed the study and wrote the manuscript. Shin Sol and Soyong Son engineered EVs. Jungmi Lee, isolated EVs. Junsik Kim, Jeongmi Lee, Sunyoung Park, Hark Kyun Kim, Seung Hyun Baek, Yoonsuk Cho, Jinsu Park, and Leon F. Palomera mainly performed the in vivo experiments. Jae Hoon Sul, Sol Shin, Jeein Lim, Jongho Kim, and Chanhee Kim conducted in vivo and ex vivo biodistribution. Jihoon Han analyzed mouse brain samples. Junsik Kim, Donghoon Ahn, Ka Young Chung, Tae-in Kam, and Yunjong Lee purified  $\alpha$ -synuclein and prepared  $\alpha$ -Syn-PFF. Seungsu Han, Jeongyun Kim, and Sangho Lee performed a bio-layer interferometry assay.

## ACKNOWLEDGEMENTS

This research was financially supported by Basic Science Research Program through the National Research Foundation of Korea (NRF), the Ministry of Education, Science and Technology, Republic of Korea (RS-2024-00345742, RS-2024-00399237, and RS-2023-00256265), by the Korea Drug Development Fund funded by the Ministry of Science and ICT, Ministry of Trade, Industry, and Energy, and Ministry of Health and Welfare (RS-2021-DD121228, RS-2022-DD128953).

## CONFLICT OF INTEREST STATEMENT

The authors declare the following competing financial interest(s): The authors declare the following competing interests: D.-G. Jo and J. H. Park are stockholders of ExoStemTech Inc. The other authors declare no competing financial interests. The graphical abstract was created with BioRender.com.

## DATA AVAILABILITY STATEMENT

All data needed to evaluate the conclusions in the paper are presented in the main manuscript, the Supplementary Information and the Supplementary Data File.

## ORCID

Hark Kyun Kim  <https://orcid.org/0000-0003-2755-0806>

Jihoon Han  <https://orcid.org/0000-0001-5870-1414>

Jae Hyung Park  <https://orcid.org/0000-0002-5043-9455>

Dong-Gyu Jo  <https://orcid.org/0000-0003-2271-1076>

## REFERENCES

- Anraku, Y., Kuwahara, H., Fukusato, Y., Mizoguchi, A., Ishii, T., Nitta, K., Matsumoto, Y., Toh, K., Miyata, K., Uchida, S., Nishina, K., Osada, K., Itaka, K., Nishiyama, N., Mizusawa, H., Yamasoba, T., Yokota, T., & Kataoka, K. (2017). Glycaemic control boosts glucosylated nanocarrier crossing the BBB into the brain. *Nature Communications*, 8(1), 1001. <https://doi.org/10.1038/s41467-017-00952-3>
- Bahn, G., Park, J.-S., Yun, U. J., Lee, Y. J., Choi, Y., Park, J. S., Baek, S. H., Choi, B. Y., Cho, Y. S., Kim, H. K., Han, J., Sul, J. H., Baik, S.-H., Lim, J., Wakabayashi, N., Bae, S. H., Han, J.-W., Arumugam, T. V., Mattson, M. P., & Jo, D.-G. (2019). NRF2/ARE pathway negatively regulates BACE1 expression and ameliorates cognitive deficits in mouse Alzheimer's models. *Proceedings of the National Academy of Sciences*, 116(25), 12516–12523. <https://doi.org/10.1073/pnas.1819541116>
- Burbulla, L. F., Song, P., Mazzulli, J. R., Zampese, E., Wong, Y. C., Jeon, S., Santos, D. P., Blanz, J., Obermaier, C. D., Strojny, C., Savas, J. N., Kiskinis, E., Zhuang, X., Krüger, R., Surmeier, D. J., & Krainc, D. (2017). Dopamine oxidation mediates mitochondrial and lysosomal dysfunction in Parkinson's disease. *Science*, 357(6357), 1255–1261. <https://doi.org/10.1126/science.aam9080>
- Burns, J. A., Kroll, D. S., Feldman, D. E., Kure Liu, C., Manza, P., Wiers, C. E., Volkow, N. D., & Wang, G.-J. (2019). Molecular imaging of opioid and dopamine systems: Insights into the pharmacogenetics of opioid use disorders. *Frontiers in Psychiatry*, 10, 626. <https://doi.org/10.3389/fpsy.2019.00626>
- Carlsson, A., Lindqvist, M., & Magnusson, T. (1957). 3,4-Dihydroxyphenylalanine and 5-hydroxytryptophan as reserpine antagonists. *Nature*, 180(4596), 1200. <https://doi.org/10.1038/1801200a0>

- Charvin, D., Medori, R., Hauser, R. A., & Rascol, O. (2018). Therapeutic strategies for Parkinson disease: Beyond dopaminergic drugs. *Nature Reviews Drug Discovery*, 17(11), 804–822. <https://doi.org/10.1038/nrd.2018.136>
- Choi, H. C., Kyungsun, Kim, D.-H., Oh, B.-K., Yim, H., Jo, S., & Choi, C. (2022). Strategies for targeted delivery of exosomes to the brain: Advantages and challenges. *Pharmaceutics*, 14(3), 672. <https://doi.org/10.3390/pharmaceutics14030672>
- Choi, H. R., Shin, H. W., Lee, H. K., Kim, J. Y., Huh, C. H., Youn, S. W., & Park, K. C. (2010). Potential redox-sensitive Akt activation by dopamine activates Bad and promotes cell death in melanocytes. *Oxidative Medicine and Cellular Longevity*, 3(3), 219–224. <https://doi.org/10.4161/oxim.3.3.8>
- Choi, I., Zhang, Y., Seegobin, S. P., Pruvost, M., Wang, Q., Purtell, K., Zhang, B., & Yue, Z. (2020). Microglia clear neuron-released  $\alpha$ -synuclein via selective autophagy and prevent neurodegeneration. *Nature Communications*, 11(1), 1386. <https://doi.org/10.1038/s41467-020-15119-w>
- Congreve, M., de Graaf, C., Swain, N. A., & Tate, C. G. (2020). Impact of GPCR structures on drug discovery. *Cell*, 181(1), 81–91. <https://doi.org/10.1016/j.cell.2020.03.003>
- Ford, C. P. (2014). The role of D2-autoreceptors in regulating dopamine neuron activity and transmission. *Neuroscience*, 282, 13–22. <https://doi.org/10.1016/j.neuroscience.2014.01.025>
- Freed, C. R., Greene, P. E., Breeze, R. E., Tsai, W.-Y., Dumouchel, W., Kao, R., Dillon, S., Winfield, H., Culver, S., Trojanowski, J. Q., Eidelberg, D., & Fahn, S. (2001). Transplantation of embryonic dopamine neurons for severe Parkinson's disease. *New England Journal of Medicine*, 344(10), 710–719. <https://doi.org/10.1056/nejm200103083441002>
- Garcia-Martin, R., Wang, G., Brandão, B. B., Zanutto, T. M., Shah, S., Kumar Patel, S., Schilling, B., & Kahn, C. R. (2022). MicroRNA sequence codes for small extracellular vesicle release and cellular retention. *Nature*, 601(7893), 446–451. <https://doi.org/10.1038/s41586-021-04234-3>
- Gonzalez, C., Bonilla, S., Flores, A., Cano, E., & Liste, I. (2015). An update on human stem cell-based therapy in Parkinson's disease. *Current Stem Cell Research & Therapy*, 11, 561–568. <https://doi.org/10.2174/1574888x10666150531172612>
- Grabarek, Z., & Gergely, J. (1990). Zero-length crosslinking procedure with the use of active esters. *Analytical Biochemistry*, 185(1), 131–135. [https://doi.org/10.1016/0003-2697\(90\)90267-D](https://doi.org/10.1016/0003-2697(90)90267-D)
- Gurung, S., Perocheau, D., Touramanidou, L., & Baruteau, J. (2021). The exosome journey: from biogenesis to uptake and intracellular signalling. *Cell Communication and Signaling*, 19(1), 47. <https://doi.org/10.1186/s12964-021-00730-1>
- Han, H. S., Lee, H., You, D., Nguyen, V. Q., Song, D. G., Oh, B. H., Shin, S., Choi, J. S., Kim, J. D., Pan, C. H., Jo, D. G., Cho, Y. W., Choi, K. Y., & Park, J. H. (2020). Human adipose stem cell-derived extracellular nanovesicles for treatment of chronic liver fibrosis. *Journal of Controlled Release: Official Journal of the Controlled Release Society*, 320, 328–336. <https://doi.org/10.1016/j.jconrel.2020.01.042>
- Han, J., Park, H., Maharana, C., Gwon, A. R., Park, J., Baek, S. H., Bae, H. G., Cho, Y., Kim, H. K., Sul, J. H., Lee, J., Kim, E., Kim, J., Cho, Y., Park, S., Palomera, L. F., Arumugam, T. V., Mattson, M. P., & Jo, D. G. (2021). Alzheimer's disease-causing presenilin-1 mutations have deleterious effects on mitochondrial function. *Theranostics*, 11(18), 8855–8873. <https://doi.org/10.7150/thno.59776>
- Han, J., Sul, J. H., Lee, J., Kim, E., Kim, H. K., Chae, M., Lim, J., Kim, J., Kim, C., Kim, J.-S., Cho, Y., Park, J. H., Cho, Y. W., & Jo, D.-G. (2024). Engineered exosomes with a photoinducible protein delivery system enable CRISPR-Cas-based epigenome editing in Alzheimer's disease. *Science Translational Medicine*, 16(759), eadi4830. <https://doi.org/10.1126/scitranslmed.adi4830>
- Hiroshi, U., Yoshikatsu, K., Do Kyung, K., Michael, F. W., Arthit, C., Emiko, M., Anders, M. W., & Endou, H. (2002). Transport of amino acid-related compounds mediated by L-type amino acid transporter 1 (LAT1): Insights into the mechanisms of substrate recognition. *Molecular Pharmacology*, 61(4), 729. <https://doi.org/10.1124/mol.61.4.729>
- Hu, X., Pan, J., Li, Y., Jiang, Y., Zheng, H., Shi, R., Zhang, Q., Liu, C., Tian, H., Zhang, Z., Tang, Y., Yang, G.-Y., & Wang, Y. (2022). Extracellular vesicles from adipose-derived stem cells promote microglia M2 polarization and neurological recovery in a mouse model of transient middle cerebral artery occlusion. *Stem Cell Research & Therapy*, 13(1), 21. <https://doi.org/10.1186/s13287-021-02668-0>
- Jung, Y. J., Kim, H. K., Cho, Y., Choi, J. S., Woo, C. H., Lee, K. S., Sul, J. H., Lee, C. M., Han, J., Park, J. H., Jo, D. G., & Cho, Y. W. (2020). Cell reprogramming using extracellular vesicles from differentiating stem cells into white/beige adipocytes. *Science Advances*, 6(13), eaay6721. <https://doi.org/10.1126/sciadv.aay6721>
- Kalani, M. Y. S., Vaidehi, N., Hall, S. E., Trabanino, R. J., Freddolino, P. L., Kalani, M. A., Floriano, W. B., Kam, V. W. T., & Goddard, W. A. (2004). The predicted 3D structure of the human D2 dopamine receptor and the binding site and binding affinities for agonists and antagonists. *Proceedings of the National Academy of Sciences*, 101(11), 3815–3820. <https://doi.org/10.1073/pnas.0400100101>
- Kam, T. I., Mao, X., Park, H., Chou, S. C., Karuppagounder, S. S., Umanah, G. E., Yun, S. P., Brahmachari, S., Panicker, N., Chen, R., Andrabi, S. A., Qi, C., Poirier, G. G., Pletnikova, O., Troncoso, J. C., Bekris, L. M., Leverenz, J. B., Pantelyat, A., Ko, H. S., ... Dawson, V. L. (2018). Poly(ADP-ribose) drives pathologic  $\alpha$ -synuclein neurodegeneration in Parkinson's disease. *Science*, 362(6414). <https://doi.org/10.1126/science.aat8407>
- Kim, E., Kim, H. K., Sul, J. H., Lee, J., Baek, S. H., Cho, Y., Han, J., Kim, J., Park, S., Park, J. H., Cho, Y. W., & Jo, D.-G. (2024). Extracellular vesicles derived from adipose stem cells alleviate systemic sclerosis by inhibiting TGF- $\beta$  pathway. *Biomolecules & Therapeutics*, 32(4), 432–441. <https://doi.org/10.4062/biomolther.2023.191>
- Kim, H. K., Cho, J., Kim, E., Kim, J., Yang, J. S., Kim, K. C., Lee, J. Y., Shin, Y., Palomera, L. F., Park, J., Baek, S. H., Bae, H. G., Cho, Y., Han, J., Sul, J. H., Lee, J., Park, J. H., Cho, Y. W., Lee, W., & Jo, D. G. (2022). Engineered small extracellular vesicles displaying ACE2 variants on the surface protect against SARS-CoV-2 infection. *Journal of Extracellular Vesicles*, 11(1), e12179. <https://doi.org/10.1002/jev2.12179>
- Kim, S., Kim, Y.-J., Park, K. H., Huh, K. M., Kang, S.-W., Lee, C. J., & Woo, D. H. (2024). Dopamine-modified hyaluronic acid (DA-HA) as a novel dopamine-mimetics with minimal autooxidation and cytotoxicity. *Redox Biology*, 76, 103320. <https://doi.org/10.1016/j.redox.2024.103320>
- Kojima, R., Bojar, D., Rizzi, G., Hamri, G. C., El-Baba, M. D., Saxena, P., Auslander, S., Tan, K. R., & Fussenegger, M. (2018). Designer exosomes produced by implanted cells intracerebrally deliver therapeutic cargo for Parkinson's disease treatment. *Nature Communications*, 9(1), 1305. <https://doi.org/10.1038/s41467-018-03733-8>
- Lee, E. S., Sul, J. H., Shin, J. M., Shin, S., Lee, J. A., Kim, H. K., Cho, Y., Ko, H., Son, S., Lee, J., Park, S., Jo, D.-G., & Park, J. H. (2021). Reactive oxygen species-responsive dendritic cell-derived exosomes for rheumatoid arthritis. *Acta Biomaterialia*, 128, 462–473. <https://doi.org/10.1016/j.actbio.2021.04.026>
- Lee, K. S., Lee, J., Kim, H. K., Yeom, S. H., Woo, C. H., Jung, Y. J., Yun, Y. E., Park, S. Y., Han, J., Kim, E., Sul, J. H., Jung, J. M., Park, J. H., Choi, J. S., Cho, Y. W., & Jo, D. G. (2021). Extracellular vesicles from adipose tissue-derived stem cells alleviate osteoporosis through osteoprotegerin and miR-21-5p. *Journal of Extracellular Vesicles*, 10(12), e12152. <https://doi.org/10.1002/jev2.12152>
- Lee, M., Ban, J.-J., Yang, S., Im, W., & Kim, M. (2018). The exosome of adipose-derived stem cells reduces  $\beta$ -amyloid pathology and apoptosis of neuronal cells derived from the transgenic mouse model of Alzheimer's disease. *Brain Research*, 1691, 87–93. <https://doi.org/10.1016/j.brainres.2018.03.034>
- Lee, M., Ban, J. J., Kim, K. Y., Jeon, G. S., Im, W., Sung, J. J., & Kim, M. (2016). Adipose-derived stem cell exosomes alleviate pathology of amyotrophic lateral sclerosis in vitro. *Biochemical and Biophysical Research Communications*, 479(3), 434–439. <https://doi.org/10.1016/j.bbrc.2016.09.069>
- Lee, M., Liu, T., Im, W., & Kim, M. (2016). Exosomes from adipose-derived stem cells ameliorate phenotype of Huntington's disease in vitro model. *The European Journal of Neuroscience*, 44(4), 2114–2119. <https://doi.org/10.1111/ejn.13275>



- Lim, G. T., You, D. G., Han, H. S., Lee, H., Shin, S., Oh, B. H., Kumar, E. K. P., Um, W., Kim, C. H., Han, S., Lee, S., Lim, S., Yoon, H. Y., Kim, K., Kwon, I. C., Jo, D. G., Cho, Y. W., & Park, J. H. (2021). Bioorthogonally surface-edited extracellular vesicles based on metabolic glycoengineering for CD44-mediated targeting of inflammatory diseases. *Journal of Extracellular Vesicles*, 10(5), e12077. <https://doi.org/10.1002/jev2.12077>
- Lin, D., Chen, H., Xiong, J., Zhang, J., Hu, Z., Gao, J., Gao, B., Zhang, S., Chen, J., Cao, H., Li, Z., Lin, B., & Gao, Z. (2022). Mesenchymal stem cells exosomal let-7a-5p improve autophagic flux and alleviate liver injury in acute-on-chronic liver failure by promoting nuclear expression of TFEB. *Cell Death & Disease*, 13(10), 865. <https://doi.org/10.1038/s41419-022-05303-9>
- Liu, Y., Choi, C. K. K., Hong, H., Xiao, Y., Kwok, M. L., Liu, H., Tian, X. Y., & Choi, C. H. J. (2021). Dopamine receptor-mediated binding and cellular uptake of polydopamine-coated nanoparticles. *ACS Nano*, 15(8), 13871–13890. <https://doi.org/10.1021/acsnano.1c06081>
- Ma, Z., Liang, H., Hu, B., Cai, S., & Yan, D. (2023). Autophagy-regulating miRNAs: Novel therapeutic targets for Parkinson's disease (Review). *International Journal of Molecular Medicine*, 51(6), 50. <https://doi.org/10.3892/ijmm.2023.5253>
- McFarthing, K., Buff, S., Rafaloff, G., Dominey, T., Wyse, R. K., & Stott, S. R. W. (2020). Parkinson's disease drug therapies in the clinical trial pipeline: 2020. *Journal of Parkinson's Disease*, 10(3), 757–774. <https://doi.org/10.3233/JPD-202128>
- Midekessa, G., Godakumara, K., Ord, J., Viil, J., Lättেকivi, F., Dissanayake, K., Kopanchuk, S., Rinken, A., Andronowska, A., Bhattacharjee, S., Rinken, T., & Fazeli, A. (2020). Zeta potential of extracellular vesicles: Toward understanding the attributes that determine colloidal stability. *ACS Omega*, 5(27), 16701–16710. <https://doi.org/10.1021/acsomega.0c01582>
- Miedel, C. J., Patton, J. M., Miedel, A. N., Miedel, E. S., & Levenson, J. M. (2017). Assessment of spontaneous alternation, novel object recognition and limb clasping in transgenic mouse models of amyloid-beta and tau neuropathology. *Journal of Visualized Experiments : JoVE*, 00(123), 55523. <https://doi.org/10.3791/55523>
- Minakaki, G., Menges, S., Kittel, A., Emmanouilidou, E., Schaeffner, I., Barkovits, K., Bergmann, A., Rockenstein, E., Adame, A., Marxreiter, F., Mollenhauer, B., Galasko, D., Buzás, E. I., Schlötzer-Schrehardt, U., Marcus, K., Xiang, W., Lie, D. C., Vekrellis, K., Masliah, E., ... Klucken, J. (2018). Autophagy inhibition promotes SNCA/alpha-synuclein release and transfer via extracellular vesicles with a hybrid autophagosome-exosome-like phenotype. *Autophagy*, 14(1), 98–119. <https://doi.org/10.1080/15548627.2017.1395992>
- Montaser, A. B., Jarvinen, J., Löffler, S., Huttunen, J., Auriola, S., Lehtonen, M., Jalkanen, A., & Huttunen, K. M. (2020). L-type amino acid transporter 1 enables the efficient brain delivery of small-sized prodrug across the blood-brain barrier and into human and mouse brain parenchymal cells. *ACS chemical neuroscience*, 11(24), 4301–4315. <https://doi.org/10.1021/acscchemneuro.0c00564>
- Nixon, R. A. (2013). The role of autophagy in neurodegenerative disease. *Nature Medicine*, 19(8), 983–997. <https://doi.org/10.1038/nm.3232>
- Park, H., Kam, T.-I., Peng, H., Chou, S.-C., Mehrabani-Tabari, A. A., Song, J.-J., Yin, X., Karuppagounder, S. S., Umanah, G. K., Rao, A. V. S., Choi, Y., Aggarwal, A., Chang, S., Kim, H., Byun, J., Liu, J. O., Dawson, T. M., & Dawson, V. L. (2022). PAAN/MIF nuclease inhibition prevents neurodegeneration in Parkinson's disease. *Cell*, 185(11), 1943–1959. <https://doi.org/10.1016/j.cell.2022.04.020>
- Park, J., Ha, H. J., Chung, E. S., Baek, S. H., Cho, Y., Kim, H. K., Han, J., Sul, J. H., Lee, J., Kim, E., Kim, J., Yang, Y. R., Park, M., Kim, S. H., Arumugam, T. V., Jang, H., Seo, S. W., Suh, P. G., & Jo, D. G. (2021). O-GlcNAcylation ameliorates the pathological manifestations of Alzheimer's disease by inhibiting necroptosis. *Science Advances*, 7(3). <https://doi.org/10.1126/sciadv.abd3207>
- Puris, E., Gynther, M., Auriola, S., & Huttunen, K. M. (2020). L-Type amino acid transporter 1 as a target for drug delivery. *Pharmaceutical Research*, 37(5), 88. <https://doi.org/10.1007/s11095-020-02826-8>
- Qu, M., Lin, Q., Huang, L., Fu, Y., Wang, L., He, S., Fu, Y., Yang, S., Zhang, Z., Zhang, L., & Sun, X. (2018). Dopamine-loaded blood exosomes targeted to brain for better treatment of Parkinson's disease. *Journal of Controlled Release: Official Journal of the Controlled Release Society*, 287, 156–166. <https://doi.org/10.1016/j.jconrel.2018.08.035>
- Sanz-Ros, J., Romero-García, N., Mas-Bargues, C., Monleón, D., Gordevicius, J., Brooke, R. T., Dromant, M., Díaz, A., Derevyanko, A., Guío-Carrión, A., Román-Domínguez, A., Inglés, M., Blasco, M. A., Horvath, S., Viña, J., & Borrás, C. (2022). Small extracellular vesicles from young adipose-derived stem cells prevent frailty, improve health span, and decrease epigenetic age in old mice. *Science Advances*, 8(42), eabq2226. <https://doi.org/10.1126/sciadv.abq2226>
- Schweitzer, J. S., Song, B., Herrington, T. M., Park, T.-Y., Lee, N., Ko, S., Jeon, J., Cha, Y., Kim, K., Li, Q., Henchcliffe, C., Kaplitt, M., Neff, C., Rapalino, O., Seo, H., Lee, I.-H., Kim, J., Kim, T., Petsko, G. A., ... Kim, K.-S. (2020). Personalized iPSC-derived dopamine progenitor cells for Parkinson's disease. *New England Journal of Medicine*, 382(20), 1926–1932. <https://doi.org/10.1056/nejmoal1915872>
- Seung Hyun, B., So Jung, P., Jae In, J., Sung Hyun, K., Jihoon, H., Jae Won, K., Sang-Ha, B., Yuri, C., Bo Youn, C., Jin Su, P., Gahee, B., Ji Hyun, S., Doo Sin, J., Joo-Yong, L., Choon-Gon, J., Thiruma, V. A., Jongpil, K., Jeung-Whan, H., Jae-Young, K., ... Dong-Gyu, J. (2017). Inhibition of Drp1 ameliorates synaptic depression, Aβ deposition, and cognitive impairment in an Alzheimer's disease model. *The Journal of Neuroscience*, 37(20), 5099. <https://doi.org/10.1523/JNEUROSCI.2385-16.2017>
- Spillantini, M. G., Schmidt, M. L., Lee, V. M. Y., Trojanowski, J. Q., Jakes, R., & Goedert, M. (1997). α-Synuclein in Lewy bodies. *Nature*, 388(6645), 839–840. <https://doi.org/10.1038/42166>
- Stavoe, A. K. H., & Holzbaur, E. L. F. (2019). Autophagy in neurons. *Annual Review of Cell and Developmental Biology*, 35(1), 477–500. <https://doi.org/10.1146/annurev-cellbio-100818-125242>
- Suleiman, E., Mayer, J., Lehner, E., Kohlhauser, B., Katholnig, A., Batzoni, M., Damm, D., Temchura, V., Wagner, A., Uberla, K., & Vorauer-Uhl, K. (2020). Conjugation of native-like HIV-1 envelope trimers onto liposomes using EDC/Sulfo-NHS chemistry: Requirements and limitations. *Pharmaceutics*, 12(10), 979. <https://doi.org/10.3390/pharmaceutics12100979>
- Thomou, T., Mori, M. A., Dreyfuss, J. M., Konishi, M., Sakaguchi, M., Wolfrum, C., Rao, T. N., Winnay, J. N., Garcia-Martin, R., Grinspoon, S. K., Gorden, P., & Kahn, C. R. (2017). Adipose-derived circulating miRNAs regulate gene expression in other tissues. *Nature*, 542(7642), 450–455. <https://doi.org/10.1038/nature21365>
- Tian, T., Zhang, H. X., He, C. P., Fan, S., Zhu, Y. L., Qi, C., Huang, N. P., Xiao, Z. D., Lu, Z. H., Tannous, B. A., & Gao, J. (2018). Surface functionalized exosomes as targeted drug delivery vehicles for cerebral ischemia therapy. *Biomaterials*, 150, 137–149. <https://doi.org/10.1016/j.biomaterials.2017.10.012>
- Trounson, A., & McDonald, C. (2015). Stem cell therapies in clinical trials: progress and challenges. *Cell Stem Cell*, 17(1), 11–22. <https://doi.org/10.1016/j.stem.2015.06.007>
- Tu, H.-Y., Yuan, B.-S., Hou, X.-O., Zhang, X.-J., Pei, C.-S., Ma, Y.-T., Yang, Y.-P., Fan, Y., Qin, Z.-H., Liu, C.-F., & Hu, L.-F. (2021). α-synuclein suppresses microglial autophagy and promotes neurodegeneration in a mouse model of Parkinson's disease. *Aging Cell*, 20(12), e13522. <https://doi.org/10.1111/acer.13522>
- Van Deun, J., Mestdag, P., Agostinis, P., Akay, Ö., Anand, S., Anckaert, J., Martinez, Z. A., Baetens, T., Beghein, E., Bertier, L., Berx, G., Boere, J., Boukouris, S., Bremer, M., Buschmann, D., Byrd, J. B., Casert, C., Cheng, L., Cmocho, A., ... Consortium, E.-T. (2017). EV-TRACK: transparent reporting and centralizing knowledge in extracellular vesicle research. *Nature Methods*, 14(3), 228–232. <https://doi.org/10.1038/nmeth.4185>
- Vázquez-Vélez, G. E., & Zoghbi, H. Y. (2021). Parkinson's disease genetics and pathophysiology. *Annual Review of Neuroscience*, 44(1), 87–108. <https://doi.org/10.1146/annurev-neuro-100720-034518>

- Volpicelli-Daley, L. A., Luk, K. C., & Lee, V. M. (2014). Addition of exogenous alpha-synuclein preformed fibrils to primary neuronal cultures to seed recruitment of endogenous alpha-synuclein to Lewy body and Lewy neurite-like aggregates. *Nature Protocols*, 9(9), 2135–2146. <https://doi.org/10.1038/nprot.2014.143>
- Wang, J., Liu, B., Xu, Y., Yang, M., Wang, C., Song, M., Liu, J., Wang, W., You, J., Sun, F., Wang, D., Liu, D., & Yan, H. (2021). Activation of CREB-mediated autophagy by thioperamide ameliorates  $\beta$ -amyloid pathology and cognition in Alzheimer's disease. *Aging Cell*, 20(3). <https://doi.org/10.1111/acer.13333>
- Wang, J., Wang, M., Jiang, N., Ding, S., Peng, Q., & Zheng, L. (2023). Emerging chemical engineering of exosomes as “bioscaffolds” in diagnostics and therapeutics. *Genes & Diseases*, 10(4), 1494–1512. <https://doi.org/10.1016/j.gendis.2022.10.020>
- Welsh, J. A., Goberdhan, D. C. I., O'Driscoll, L., Buzas, E. I., Blenkiron, C., Bussolati, B., Cai, H., Di Vizio, D., Driedonks, T. A. P., Erdbrugger, U., Falcon-Perez, J. M., Fu, Q. L., Hill, A. F., Lenassi, M., Lim, S. K., Mahoney, M. G., Mohanty, S., Moller, A., Nieuwland, R., ... Witwer, K. W. (2024). Minimal information for studies of extracellular vesicles (MISEV2023): From basic to advanced approaches. *Journal of Extracellular Vesicles*, 13(2), e12404. <https://doi.org/10.1002/jev2.12404>
- Woo, C. H., Kim, H. K., Jung, G. Y., Jung, Y. J., Lee, K. S., Yun, Y. E., Han, J., Lee, J., Kim, W. S., Choi, J. S., Yang, S., Park, J. H., Jo, D. G., & Cho, Y. W. (2020). Small extracellular vesicles from human adipose-derived stem cells attenuate cartilage degeneration. *Journal of Extracellular Vesicles*, 9(1), 1735249. <https://doi.org/10.1080/20013078.2020.1735249>
- Yamanaka, S. (2020). Pluripotent stem cell-based cell therapy—promise and challenges. *Cell Stem Cell*, 27(4), 523–531. <https://doi.org/10.1016/j.stem.2020.09.014>
- Yang, J., Luo, S., Zhang, J., Yu, T., Fu, Z., Zheng, Y., Xu, X., Liu, C., Fan, M., & Zhang, Z. (2021). Exosome-mediated delivery of antisense oligonucleotides targeting alpha-synuclein ameliorates the pathology in a mouse model of Parkinson's disease. *Neurobiology of Disease*, 148, 105218. <https://doi.org/10.1016/j.nbd.2020.105218>
- Yin, J., Chen, K. M., Clark, M. J., Hijazi, M., Kumari, P., Bai, X. C., Sunahara, R. K., Barth, P., & Rosenbaum, D. M. (2020). Structure of a D2 dopamine receptor-G-protein complex in a lipid membrane. *Nature*, 584(7819), 125–129. <https://doi.org/10.1038/s41586-020-2379-5>
- Zhang, H., Jiang, Y., Zhao, S.-G., Jiang, L.-Q., Meng, Y., Liu, P., Kim, M. O., & Li, S. (2015). Selective neuronal targeting, protection and signaling network analysis via dopamine-mediated mesoporous silica nanoparticles. *MedChemComm*, 6(6), 1117–1129. <https://doi.org/10.1039/c5md00038f>
- Zhuang, Y., Xu, P., Mao, C., Wang, L., Krumm, B., Zhou, X. E., Huang, S., Liu, H., Cheng, X., Huang, X. P., Shen, D. D., Xu, T., Liu, Y. F., Wang, Y., Guo, J., Jiang, Y., Jiang, H., Melcher, K., Roth, B. L., ... Xu, H. E. (2021). Structural insights into the human D1 and D2 dopamine receptor signaling complexes. *Cell*, 184(4), 931–942e918. <https://doi.org/10.1016/j.cell.2021.01.027>

## SUPPORTING INFORMATION

Additional supporting information can be found online in the Supporting Information section at the end of this article.

**How to cite this article:** Sul, J. H., Shin, S., Kim, H. K., Han, J., Kim, J., Son, S., Lee, J., Baek, S. H., Cho, Y., Lee, J., Park, J., Ahn, D., Park, S., Palomera, L. F., Lim, J., Kim, J., Kim, C., Han, S., Chung, K. Y., ... Jo, D.-G. (2024). Dopamine-Conjugated Extracellular Vesicles Induce Autophagy in Parkinson's Disease. *Journal of Extracellular Vesicles*, 13, e70018. <https://doi.org/10.1002/jev2.70018>